Hardware Design for In-Mine Positioning System

A Thesis Submitted

to the College of Graduate Studies and Research

in Partial Fulfillment of the Requirements

for the Degree of Master of Science

in the Department of Electrical Engineering

University of Saskatchewan

Saskatoon, Saskatchewan

by

Abu Maqsud

PERMISSION TO USE

In presenting this thesis in partial fulfillment of the requirements for a Postgraduate degree from the University of Saskatchewan, it is agreed that the Libraries of this University may make it freely available for inspection. Permission for copying of this thesis in any manner, in whole or in part, for scholarly purposes may be granted by the professors who supervised this thesis work or, in their absence, by the Head of the Department of Electrical Engineering or the Dean of the College of Graduate Studies and Research at the University of Saskatchewan. Any copying, publication, or use of this thesis, or parts thereof, for financial gain without the written permission of the author is strictly prohibited. Proper recognition shall be given to the author and to the University of Saskatchewan in any scholarly use which may be made of any material in this thesis.

Request for permission to copy or to make any other use of material in this thesis in whole or in part should be addressed to:

Head of the Department of Electrical Engineering

57 Campus Drive

University of Saskatchewan

Saskatoon, Saskatchewan, Canada

S7N 5A9

i

ACKNOWLEDGMENTS

UNIVERSITY OF SASKATCHEWAN

Electrical Engineering Abstract

Hardware Design for In-Mine Positioning System

Student: Abu Maqsud

Supervisor: Prof. Brian Daku

M.Sc. Thesis Submitted to the

College of Graduate Studies and Research

2008

ABSTRACT

This thesis describes the hardware design of a positioning system which locates a vehicle relative to a digital map of an underground mine. The mines of interest are potash mines of Saskatchewan, and they are at a depth of approximately 1000 meters and they cover an area larger than 10 kilometers by 10 kilometers. An important application of an in-mine positioning system is tracking a ground penetrating radar system. Ground penetrating radar is used to determine the current condition of the mine ceiling and to evaluate its risk of delamination. A ground penetrating radar system is driven along a mine tunnel and measurements are logged. It is necessary to record position information along with the radar signal and this can be done with the aid of a positioning system.

The design and evaluation of the hardware system that supports a positioning system, which can locate a vehicle inside a mine tunnel with reasonable accuracy and cost is described in this thesis. The hardware system includes a dead reckoning system

(DRS), which is built using MEMS (Micro Electro Mechanical System) accelerometer and gyroscope sensors and ultrasonic distance sensors, along with a data acquisition system.

Table of Contents

List of Figures

List of Tables

List of Abbreviations

2D	2-Dimensional
3D	3-Dimensional
A/D	Analog to Digital converter
BW	Bandwidth
DAQ	Data Acquisition
dB	decibels
DoD	Department of Defence,USA
DRS	Dead Reckoning System
ENOB	Effective Number of Bits
GPR	Ground Penetrating Radar
GPS	Global Positioning System
JPO	Joint Program Office
LSB	Least Significant Bit
MEMS	Micro Electro Mechanical System
MMS	Minimum Mean Square
OBDII	On-Board Diagnostic systems
PDF	Probability Density Function
PF	Particle Filter
PSD	Power Spectral Density
RF	Radio Frequency
RMS	Root Mean Square
SNR	Signal to Noise Ratio
SQNR	Signal-to-Quantization Noise Ratio

1. Introduction

A positioning system is defined as a system that locates a mobile object relative to a reference coordinate system. For example, the Global Positioning System (GPS) uses signals from orbiting satellites to locate a mobile receiver on the earth's surface. GPS requires line-of-sight between the receiver and the orbiting satellites and thus cannot be used near large buildings, in tunnels or in underground mines. This research focuses on locating mobile objects in structures with no access to GPS signals. The specific application area is underground potash mines.

Potash mines produce potash salts, and potassium, which is a major component in most commercial fertilizers, is extracted from potash salts. Typical Saskatchewan potash mines are at a depth of approximately 1000 meters and these mines are relatively large being greater than 10 kilometer by 10 kilometers. They consist of a set of interconnected straight tunnels that are referred to as rooms. These rooms are produced by large mining machines which extract the ore. An example of a mining machine used to extract ore is shown in Figure 1.1.

Once a mining machine has extracted the ore, creating a room, there is some small risk that the room ceiling will delaminate and thus collapse. Delamination could occur for many reasons including geological anomalies. If geological anomalies can be detected, delamination of mine ceiling can be predicted in advance. One technique that is used to detect geological anomalies is surveying with Ground Penetrating Radar (GPR) [1]. The GPR uses electromagnetic wave propagation and scattering to image, locate and quantitatively identify changes in electrical and magnetic properties

1

Figure 1.1: A mining machine excavating tunnels through underground mines

in the ground and thus detect the geological anomalies. These collected data need to be correlated with the position of the GPR in the potash mine. Thus one application of the proposed positioning system is to locate the GPR vehicle relative to the mine map.

The proposed positioning system, which is applicable to underground potash mines, can be used in other underground mines or tunnel type structures, including train and automotive tunnels to locate vehicles [2].

1.1   In-Mine Positioning System

The in-mine positioning system needs to determine the location, or coordinates of a mobile object, such as a vehicle, in an underground mine with reasonable accuracy and cost.   A block diagram of the proposed in-mine positioning system is shown
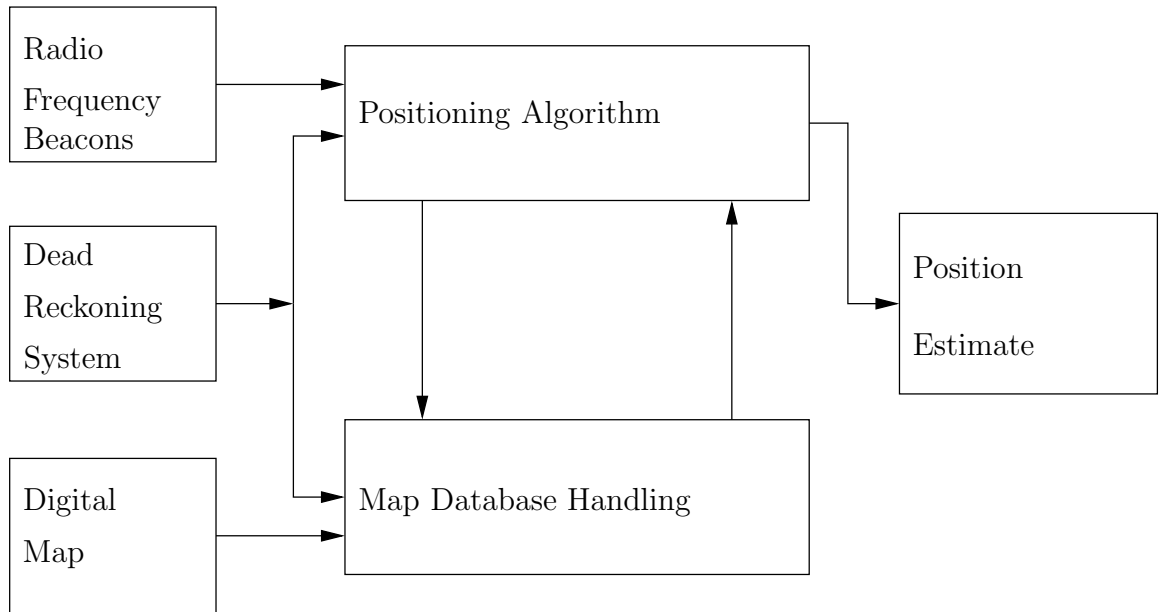
Figure 1.2: Block diagram of the proposed mine positioning system

in Figure 1.2.   The proposed positioning system needs an estimate of the initial position relative to the mine map and the radio frequency (RF) reference beacons are used to serve this purpose.   The RF receiver, which is attached to the vehicle, will receive an estimate of the initial location from the RF reference beacons located at the entrance of the mine.   Additional RF reference beacons can be placed at key locations throughout the mine to provide additional references relative to the mine map.   Besides the information on the initial position of the vehicle, the positioning system also needs information on the relative position of the vehicle.   In order to calculate the relative position, the system integrates data from an attached dead

reckoning system (DRS). A DRS estimates relative position of the vehicle as the vehicle moves away from a known position. The relative position is estimated using various types of inertial sensors in order to gather information such as course, speed, time and distance that the vehicle travels. The positioning system also needs a relative reference frame such a mine map similar to Figure 1.3, where the lines on the map
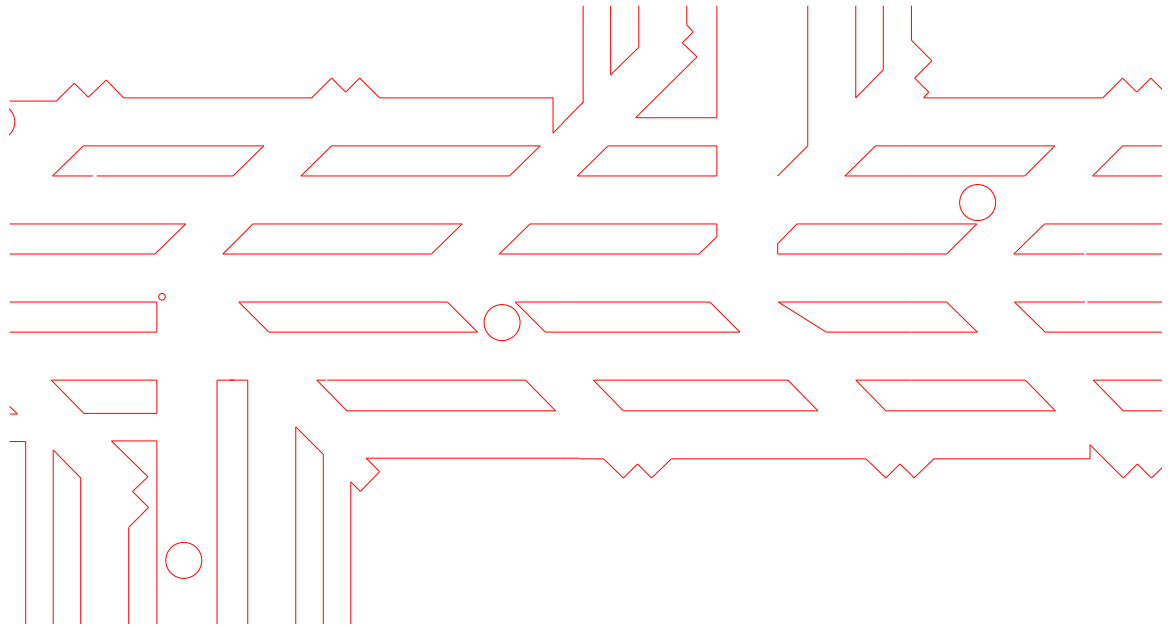
Figure 1.3: An example of a section of a mine map

indicate mine tunnels. An estimate of the location of a vehicle inside the underground mine is obtained by combining the data from the dead reckoning system, the radio frequency reference beacons and the digital mine map information using a statistical data fusion algorithm.

4

1.2 Thesis Objective

The main objective of this thesis is to describe the design and the evaluation of the hardware system that supports a positioning system, which can locate a mobile object such as a vehicle inside a mine tunnel relative to a mine map with a reasonable accuracy of 1 meter and cost less than $1000. The system should require minimum installation time and effort. The hardware system includes a dead reckoning system (DRS). Recent accelerometers and gyroscopes implemented using MEMS (Micro Electro Mechanical System) technology have lowered the cost of this system significantly. A dead reckoning system using these types of MEMS sensors along with ultrasonic distance sensors is built and tested.

The detailed discussion and the process of implementation of the positioning algorithm, RF beacons and digital mine maps are outside the scope of this thesis, and is part of future work that will be presented in another thesis.

1.3 Thesis Outline

Chapter two of this thesis provides an overview of the proposed positioning system and its three main blocks: the dead reckoning system, the algorithm and the radio frequency reference beacons.

Chapter three describes the design of the dead reckoning system and the use of data acquisition system to collect sensor data. It also describes different evaluation test setups and discusses experimental results.

Chapter four discusses the integration of the sensor data and the evaluation of the dead reckoning system. It describes an example test run inside a tunnel-like structure. This chapter also compares experimental sensor data with the expected data.

Chapter five gives an overall summary of the thesis, it also discusses the findings in this research and makes recommendations for further improvements.

2. In-Mine Positioning System

In chapter one, one possible application of an in-mine positioning system, which involves locating a ground penetrating radar system was discussed. This chapter gives a general description of the proposed solution and an overview of the different parts of the system.

2.1 Proposed Positioning System

In today's Global Positioning System (GPS) dependent world, some have the notion that navigation and positioning are simply and almost solely accomplished through the use of GPS. While GPS is and will continue to be an excellent positioning system, it is neither flawless nor is it the only system employed in positioning. Moreover in a mine tunnel, GPS satellite signals cannot be received. Therefore, an alternative positioning system is needed. The proposed positioning system must have reasonable accuracy of 1 m and an affordable price less than $1000. In addition, the operational environment in an underground mine can be harsh because of the heat and salt dust. Thus any manufactured product would have to operate under these conditions though these environmental issues are not addressed in this thesis.

The proposed positioning system has four main parts and they are:

1. Radio Frequency Reference Beacons

2. Dead Reckoning System

3. Digital Mine Map, and

4. Algorithm

The positioning system integrates information from the radio frequency (RF) reference beacons, which give an estimate of the initial position, information from a dead reckoning system (DRS), which gives the relative position compared to a known initial position, and the information from the digital mine map. This information is integrated using a data fusion algorithm that is based on a map matching statistical positioning technique to locate an object in an underground mine.

2.2   Radio Frequency (RF) Reference Beacon

The goal of the Radio Frequency (RF) reference beacon is to provide the initial estimate of the position of a mobile object. It also can be used to provide a reference position in a limited number of locations throughout the mine. Since the RF system is outside the scope of this thesis, a detailed description is omitted.

2.3   Dead Reckoning (DR) System

Dead reckoning is the process of estimating the position of an object by advancing a known position using course, speed, and time that the object traveled. That is, in other words, calculating where the object momentarily is at a certain time if the object held the speed, time and course as it traveled [3].

Dead reckoning (DR) is a method of navigation used for many years in numerous applications on variety of mobile objects such as ships, aircraft, trucks, cars, rail engines, and more recently, mobile robots. Thus design specifications and implementations change depending on the application. The following section describes the background concept of a dead reckoning system and its application to an in-mine positioning system.

2.3.1 Dead Reckoning Background

A simple one-dimensional example of positioning involves the determination of the position of an object, which is moving along a track between two locations on a perfectly flat plane. It is possible to determine the instantaneous speed of the object and distance it has traveled from a known starting point by using measurements of its acceleration along the track. Sensors called accelerometers provide such information. If an accelerometer is fixed to the object, it will provide information about the acceleration of the object. The time integral of the acceleration measurement provides a continuous estimate of the instantaneous velocity of the object, provided that the initial velocity was known. A second integration yields the distance traveled with respect to a known starting point. The accelerometer together with a computer capable of integration makes a simple one dimensional dead reckoning system.

An one dimensional dead reckoning system needs to determine the location of an object in terms of x coordinates in a reference frame as it is shown in Figure 2.1 for an object moving with a fixed direction.

Object

Fixed track

Reference Frame   Instantaneous x position
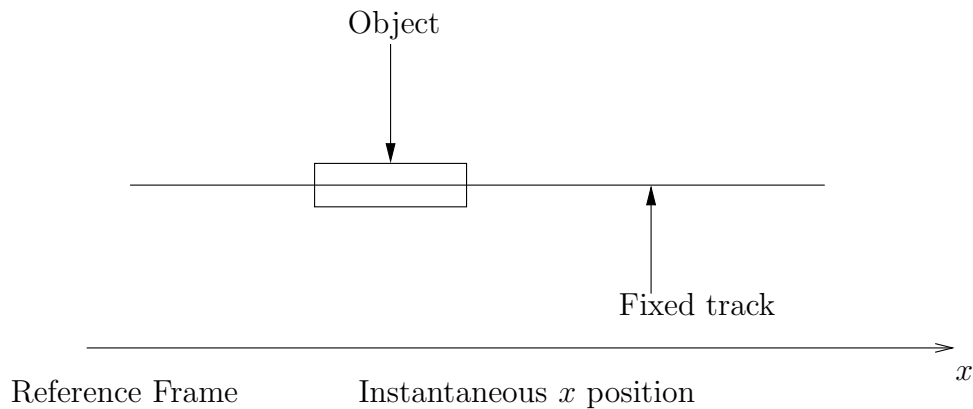
Figure 2.1: One-dimensional dead reckoning

For the more general situation, illustrated in Figure 2.2, where there is no fixed

track, it is necessary to detect continuously the motion of the object in three per-
pendicular directions (X, Y, Z) and also the rotational motions, which are known as
roll (about X axis), pitch (about Y axis), and yaw or bearing (about Z axis). Three
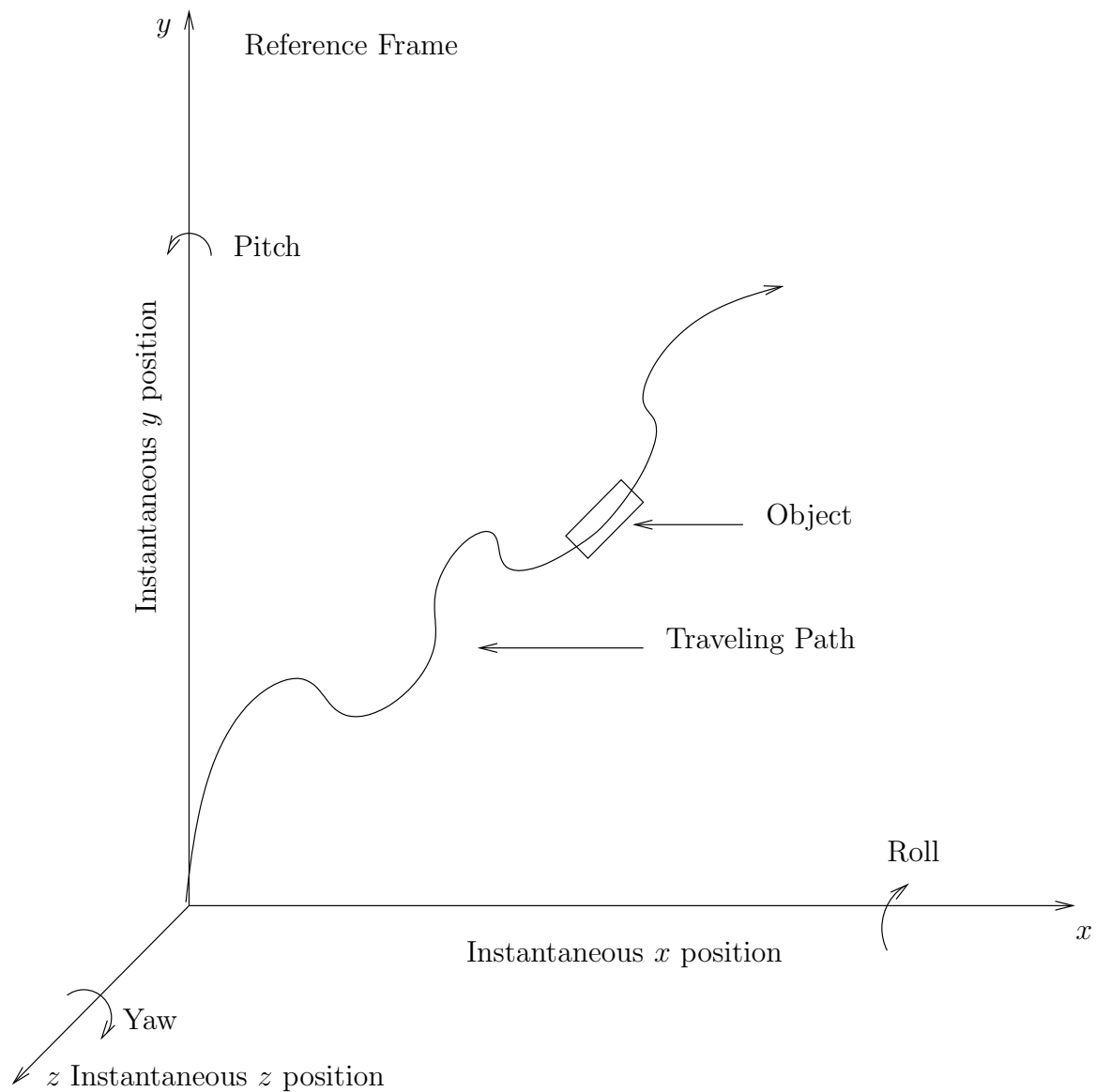
Figure 2.2: Three-dimensional dead reckoning

accelerometers are required to detect the motion in three perpendicular directions.
One sensor suitable for measuring the rotational motion about an axis perpendicular

to the plane of motion is a gyroscope. Depending on the construction of this sensor, it may be used to provide either a direct measurement of the object's heading relative to the reference frame or a measurement of the turn rate of the object. In the latter case, the angular orientation of the object is calculated by the integration of this measurement, provided the angle is known at the start of the travel. Given such information, it is possible to relate the measurements to the reference frame. The instantaneous measurements may therefore be resolved in the reference frame and integrated with respect to time to determine the instantaneous velocity and position of the vehicle with respect to that frame. Therefore it is possible to construct a simple three-dimensional dead reckoning system using three gyroscopes, three accelerometers and a computer with integration facilities. It must be mentioned that the dead reckoning system is fundamentally dependent on an accurate knowledge of position, speed and heading being available prior to start of traveling.

Examples of many existing dead reckoning systems can be given. The design of a dead reckoning system changes with applications, constraints and costs. Today's aircrafts and ships use sophisticated dead reckoning systems for their positioning and navigation systems. The dead reckoning system assists in flying and navigation of an aircraft. Usually a dead reckoning system for an aircraft has three gyroscopes: an altitude indicator gyroscope (vertical gyroscope), a direction indicator gyro, and a turn and bank indicator gyroscope and three accelerometers. Commercial aircraft such as Boeing 767 and 757 and combat fighter plane such as F-16 Fighting Falcon, combine a global positioning system with a ring laser gyroscope inertial navigation system, to provide pilots with a more reliable, precision navigation system [4]. The ring laser gyroscope is a highly accurate way to measure changes in angular position. The ring laser gyroscope has extremely low drift of 0.0001°/hour [3]. But the draw back is that perfect quality glass machined cavities, precision mirrors, high voltages

(> 1 kV), lasers and inert gases are all required to build a ring laser gyroscope. The resulting system is well over \$100000 [5]. Aircraft also keep track of the distance from the land. In order to measure the distance from land, some aircraft use Distance Measuring Equipment (DME). This DME is a transponder-based radio navigation technology to determine distance from a land-based transponder by sending and receiving pulse pairs and by timing the propagation delay of ultra high frequency radio signals.

These are just few examples of the many kinds of dead reckoning systems. These variety of dead reckoning systems are designed depending on the needs and applications. A dead reckoning system which best suits the need of an affordable (cost less than \$1000) in-mine positioning system is proposed in the next section.

2.3.2 DRS for In-Mine Positioning

Inside mine tunnels, where GPS signals cannot be received and radio signals will cause multi-path error, a dead reckoning system (DRS) is the most feasible and cost effective positioning system. Having an estimate of the initial position, through radio frequency reference beacons, the system can calculate the vehicle's current position. The proposed DRS for the in-mine positioning system uses a combination of MEMS accelerometer and gyroscope sensors.

The physical constraints in an underground mine can be used to simplify the dead reckoning system. It is assumed that mine floors do not tilt about the x axis and there is no roll angle. Moreover, the location of a vehicle in a mine can be given in terms of a two dimensional co-ordinate system by taking a top view of a mine map and projecting the vehicle onto it according to the distance traveled in x and y directions. But to measure the projected x and y distances, the dead reckoning system must be capable of measuring the distance traveled in the vertical (z) direction as well, since

the vehicle might go through upward or downward slopes.

Another physical constraint that can be used to further enhance the positioning system is the distance to the side wall. The majority of the mine rooms have limited width (less than 10 meter) and the distance to the mine walls can be measured using ultrasound sensors. Measured distances from the side walls are combined with the accelerometer and the gyroscope information using the positioning algorithm to locate the vehicle relative to a the mine map.

Considering the physical constraints, the dead reckoning system can be implemented with a dual axis accelerometer, a single axis gyroscope and two ultrasound distance sensors, all of which are attached rigidly to the body of the vehicle. In addition, speed data could be calculated from the vehicle's OBDII (On-Board Diagnostic) interface, if available [6]. Usually a vehicle such a Jeep is used to carry the GPR system and this vehilce will have an OBDII interface if it is a 1996 or newer vehicle.

A block diagram of the dead reckoning system is given in Figure 2.3. The vehicle's body is represented in Figure 2.3 by the block on which the sensors and other instruments are mounted. The two sensitive axes of the dual axis accelerometer, indicated by the direction of the arrows in the diagram, are at right angle to one another and aligned with the body axes of the object; they are denoted as a_f and a_d, the acceleration in the forward and the vertical directions respectively. The gyroscope is mounted with its sensitive axis aligned to the forward direction allowing it to detect rotations (bearing, θ) about an axis perpendicular to the plane of motion; the vertical axis.

It is assumed that the position is calculated with respect to a space-fixed reference frame denoted by the axes x and y. The coordinate of the object's body from a known

starting point x_i, y_i could be determined by translating (T) forward and vertical direction accelerations a_f, a_d and bearing θ into absolute reference frame as a_x and a_y and by double integrating after addition of initial speed v_{xi}, v_{yi} and initial position x_i, y_i in the respective directions. Distance from the left side wall, m_l and distance from the right side wall, m_r are measured by ultrasound sensors. Figure 2.3 shows a possible method for obtaining the position, though in a noisy environment with non-ideal sensors this approach is not feasible. The actual position will be obtained using the algorithm in Section 2.5.
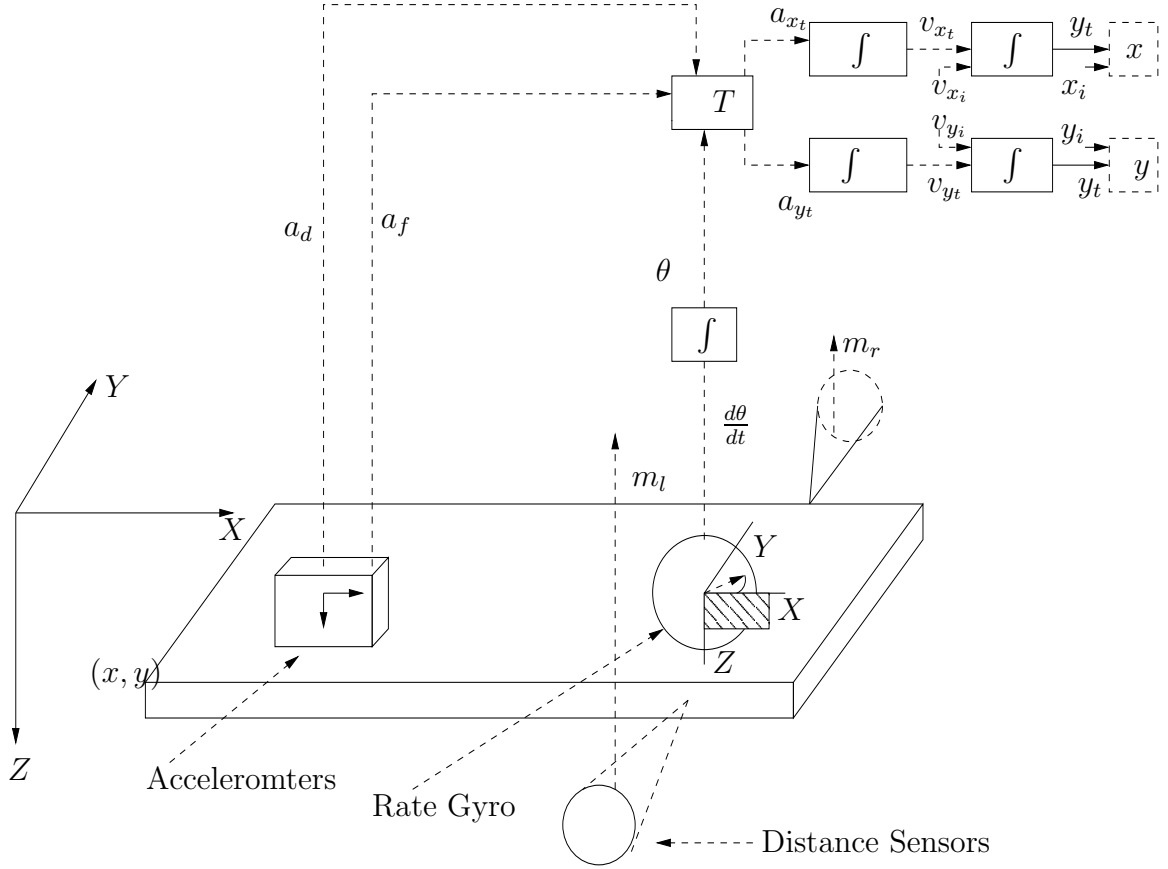
Figure 2.3: Dead reckoning system for in-mine positioning system

Details of the design and evaluation of the dead reckoning sensor system hardware

will be given in following chapters.

2.4 Digital Mine Map

A digital mine map is provided and is used to find the location of a vehicle relative to the mine map. Various computer aided drawing (CAD) software programs are used to specify mine maps. These maps are created from survey points when mines are originally cut and their precision range is ± 2 cm. A digital map database can be constructed from the CAD specified mine maps. A map database handling program makes information such as distance to side walls from a particular location available to the positioning algorithm.

2.5 Algorithm

A significant component of the positioning system is an optimal real time algorithm that can combine the disparate sources of data from the various positioning sensors to determine the position of the vehicle relative to the digital map of the area. These types of algorithms are typically referred to as data fusion or sensor fusion algorithms. The algorithm for the positioning system for vehicles inside mine tunnels will use advanced nonlinear filtering techniques and will combine information from the dead reckoning system and a digital map. Given a rough estimate of the initial position, the statistical data fusion algorithm will be able to estimate the position of the vehicle as the vehicle moves. Relative position information is observed through a dead reckoning system.

A possible algorithm is a recursive Bayesian estimation algorithm [7]. From the statistical point of view, the knowledge about the vehicle's position at each time instant is completely summarized by the conditional probability density function (PDF). The PDF evolves with time and information received from the system sen-
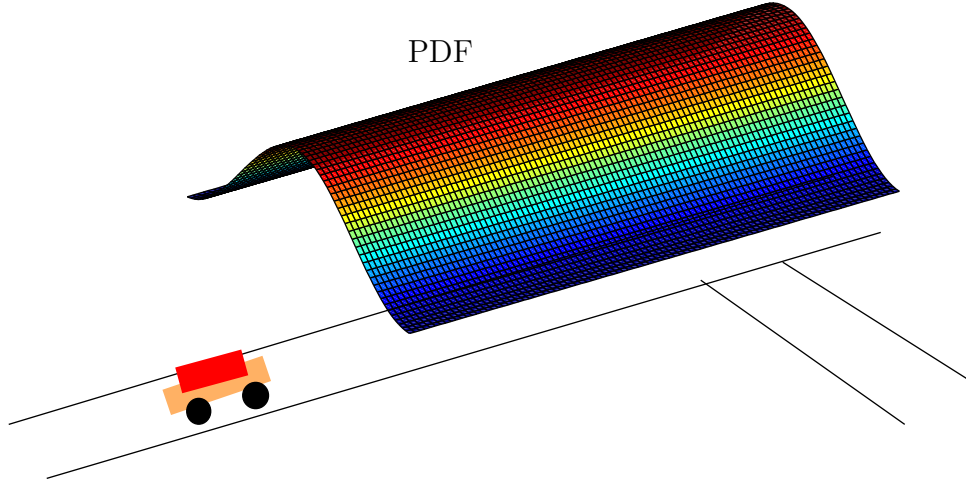
Figure 2.4: The PDF is distributed along the straight tunnel [8]

sors [8]. Estimation of the position is done by finding the expectation.

An example can be drawn for a two dimensional case. Assume that a vehicle is traveling along a straight tunnel with a known initial position. The vehicle's position will have a PDF distributed along the tunnel similar to Figure 2.4. If the vehicle later makes a turn to a tunnel at the right, the additional information about the movement and the spatial configuration of the map produces a better estimate of the position as indicated in the PDF of Figure 2.5. The consequence is that the mass of the PDF gets concentrated about the actual position of the vehicle.
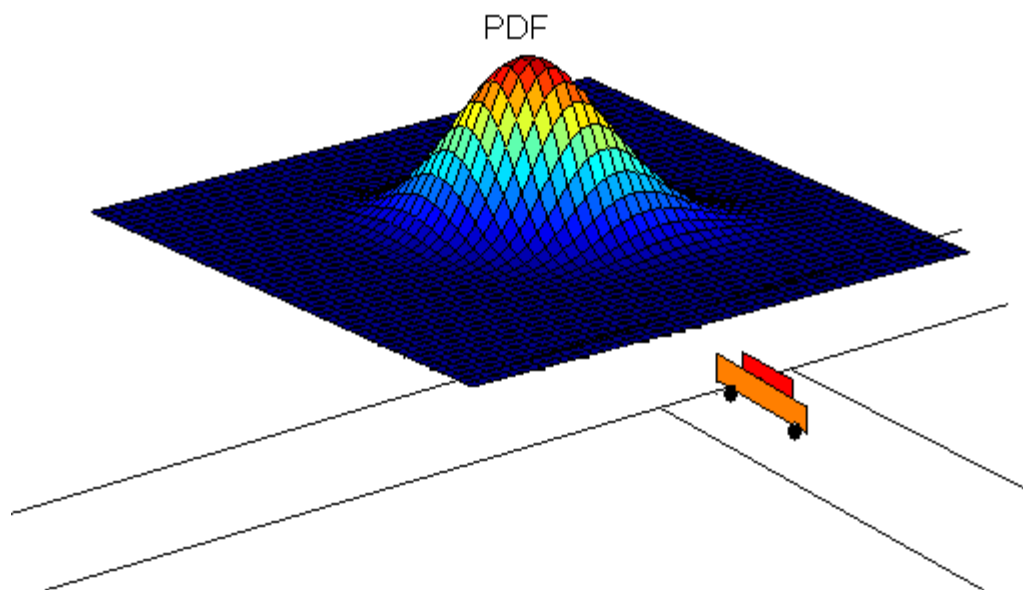
Figure 2.5: The PDF is concentrated with a peak after making a turn [8]

2.5.1 State Space Model

The proposed system is modelled as a nonlinear discrete-time state space system. In the proposed system, two models are needed to make an inference about a dynamic system: a system model and a measurement model [9, 10]. The system model describes the system's state as it evolves in time and the measurement model relates measurement with the state. The general form of the state equation is:

$$X_{k+1} = f(X_k, U_k) + W_k \tag{2.1}$$

where the state vector

$$X = [x, y, s, \theta, \phi, \delta_{a_f}, \delta_{a_d}]^T \tag{2.2}$$

where x is the x coordinate, y is the y coordinate, s is vehicle's speed in the direction of travel, θ is the bearing from the $x - z$ plane, ϕ is the pitch from the $x - y$ plane, δ_{a_f} is the acceleration bias in the forward direction, δ_{a_d} is the acceleration bias in the downward direction and T denotes the transpose operator. The state vector X represents the object's position and orientation on the map. The input vector

$$U = [a_f, a_d, \dot{\theta}]^T \tag{2.3}$$

where a_f is the acceleration in the forward direction, a_d is the acceleration in the downward direction and $\dot{\theta}$ is the rate of change of bearing, θ. In equation (2.1), W is the process noise vector and the added subscript to each vector indicates the time series iteration, with k representing the current sample. After each iteration, the state vector X_k is updated.

Expanding the functional relationship in equation (2.1) and by applying physics and geometry to the available sensor data, the following set of state update equations can be defined.

$$
\begin{aligned}
x_{k+1} = {} & x_k + s_k T_s \cos\theta_k \cos\phi_k + \tfrac{T_s^2}{2}\delta_{a_{f(k)}} \cos\theta_k \cos\phi_k \\
& + \tfrac{T_s^2}{2}(a_{f(k)} - g\sin\phi_k)\cos\theta_k \cos\phi_k + w_{1(k)}
\end{aligned} \tag{2.4}
$$

18

$$y_{k+1} = y_k + s_k T_s \sin\theta_k \cos\phi_k + \frac{T_s^2}{2}\delta_{a_{f(k)}} \sin\theta_k \cos\phi_k$$
$$+ \frac{T_s^2}{2}(a_{f(k)} - g\sin\phi_k)\sin\theta_k \cos\phi_k + w_{2(k)} \tag{2.5}$$

$$s_{k+1} = s_k + T_s(\delta_{a_{f(k)}} + a_{f(k)} - g\sin\phi_k) + w_{3(k)} \tag{2.6}$$

$$\theta_{k+1} = \theta_k + T_s\dot{\theta}_k + w_{4(k)} \tag{2.7}$$

$$\phi_{k+1} = \arccos\frac{a_{d(k)}}{g} + w_{5(k)} \tag{2.8}$$

$$\delta_{a_{f(k+1)}} = \delta_{a_{f(k)}} + w_{6(k)} \tag{2.9}$$

$$\delta_{a_{d(k+1)}} = \delta_{a_{d(k)}} + w_{7(k)} \tag{2.10}$$

where T_s is the sampling period and $g = 9.81$ m/s^2 is gravitational acceleration.

The distance to the tunnel walls are measured using ultrasonic sensors and are represented by the measurement vector,

$$M = [m_l, m_r]^T \tag{2.11}$$

where m_l is the measured distance to the left wall and m_r is the measured distance to the right wall. The measurement equation is

$$M_k = D_k + V_k \tag{2.12}$$

where V is the measurement noise vector and

$$D = [d_l, d_r]^T \tag{2.13}$$

with d_l and d_r being the estimated distance to the left side wall and to the right side wall. D is calculated using $D = g(X, \text{map})$, where the function $g(\cdot)$ gives the distance from the estimated position defined by X to the walls defined by the digital map.

There are many methods to solve the equations, (2.1) and (2.12) and all are based on what are known as Bayes Filters [11] and their differences lie in how the

19

probability densities are represented. Recursive Bayes Filters in general make use of the Markov assumption. That is, the measurements M_k and input U_k are conditionally independent of the state X_k and past measurements.

With this assumption, the posterior density for the current state can be calculated with only knowledge of the previous posterior density and current measurements and inputs.

The posterior probability density, which is known as the belief, $Bel(X_k)$, is

$$Bel(X_k) = p(X_k|M_k, U_k, M_{k-1}, U_{k-1}, ..., M_0, U_0) \tag{2.14}$$

The current belief can be calculated using only the current measurements, current inputs and the previous belief as follows. First, define

$$Bel^-(X_k) = \int p(X_k|X_{k-1})Bel(X_{k-1}dX_{k-1}) \tag{2.15}$$

This can be used to update the current belief

$$Bel(X_k) = \alpha p(M_k|X_k)Bel^-(X_k) \tag{2.16}$$

where α is a normalization constant to ensure it is a true probability density.

As mentioned above, the difference between the types of filters lie in how they represent the densities in the equations (2.15) and (2.16). One such filter is Particle Filter and the proposed system will likely use this filter.

2.5.2   Particle Filter

Particle filters are Sequential Monte Carlo methods typically used with non-linear systems or with systems corrupted by non-Gaussian noise. A Particle filter is also called a recursive Bayesian estimation algorithm and it is used to estimate the conditional probability density of user position given the measurements and inputs at

each time instant. A particle filter represents the PDF by a set of particles, each with corresponding weight, or importance value.

There are three majors steps to a particle filter algorithm:

1. generation of particles (sample),

2. computation of particle weights (importance), and

3. re-sampling

Particle Generation

Particle generation is also referred to as sampling. In this step, samples are generated using the state equations and the state from the previous time step, which is already resampled. For the initial particle generation a random set of samples is generated. This step uses the following sampling equations that are based on the state update equations, where the superscript $n = 1$ to N is the particle number.

$$
\begin{aligned}
x_{k+1}^{(n)} = \ & x_k^{(n)} + s_k^{(n)} T_s \cos\theta_k^{(n)} \cos\phi_k^{(n)} + \frac{T_s^2}{2} \delta_{a_{f(k)}}^{(n)} \cos\theta_k^{(n)} \cos\phi_k^{(n)} \\
& + \frac{T_s^2}{2}(a_{f(k)}^{(n)} - g\sin\phi_k^{(n)}) \cos\theta_k^{(n)} \cos\phi_k^{(n)} + w_{1(k)}
\end{aligned}
\tag{2.17}
$$

$$
\begin{aligned}
y_{k+1}^{(n)} = \ & y_k^{(n)} + s_k^{(n)} T_s \sin\theta_k^{(n)} \cos\phi_k^{(n)} + \frac{T_s^2}{2} \delta_{a_{f(k)}}^{(n)} \sin\theta_k^{(n)} \cos\phi_k^{(n)} \\
& + \frac{T_s^2}{2}(a_{f(k)}^{(n)} - g\sin\phi_k^{(n)}) \sin\theta_k^{(n)} \cos\phi_k^{(n)} + w_{2(k)}
\end{aligned}
\tag{2.18}
$$

$$
s_{k+1}^{(n)} = \ s_k^{(n)} + T_s(\delta_{a_{f(k)}}^{(n)} + a_{f(k)}^{(n)} - g\sin\phi_k^{(n)}) + w_{3(k)}
\tag{2.19}
$$

$$
\theta_{k+1}^{(n)} = \theta_k^{(n)} + T_s \dot{\theta}_k^{(n)} + w_{4(k)}
\tag{2.20}
$$

$$
\phi_{k+1}^{(n)} = \arcsin \frac{a_{d(k)}^{(n)}}{g} + w_{5(k)}
\tag{2.21}
$$

$$
\delta_{a_{f(k+1)}}^{(n)} = \delta_{a_{f(k)}}^{(n)} + w_{6(k)}
\tag{2.22}
$$

$$
\delta_{a_{d(k+1)}}^{(n)} = \delta_{a_{d(k)}}^{(n)} + w_{7(k)}
\tag{2.23}
$$

21

Importance Weight Calculation

After the state has been sampled, the importance weights need to be calculated and normalized. The importance weights are calculated using:

$$q_k^{*(n)} = q_{k-1}^{(n)} e^{-0.5\left(M_k^{(n)} - D_k\right)^T R^{-1}\left(M_k^{(n)} - D_k\right)} \tag{2.24}$$

for $n = 1,2,...,N$. Where, R is the covariance for measurement noise vector, V, and R is assumed to be a diagonal matrix with common variance terms. Terms from the Gaussian density are not included in equation (2.24) since they cancel in equation (2.25).

The weights are normalized by

$$q_k^{(n)} = \frac{q_k^{*(n)}}{\sum_{m=1}^{N} q_k^{*(m)}} \tag{2.25}$$

for $n=1,2,...N$.

Resample

Re-sampling improves the estimation of future states by concentrating particles into domains of higher posterior probability. It is a tool used to avoid degeneracy since the variance of the importance weights increases with time for sequential importance sampling methods. There are several methods of re-sampling such as Residual Re-sampling (RR) and Systematic Re-sampling (SR) [12]. For the proposed positioning system, the Systematic Re-sampling algorithm, which will be discussed in another thesis, is used.

Output

The estimate of the state values can be calculated using the expected value or by determining the maximum a posteriori (MAP) estimate. The expectation is calculated as the sum over all particles weighted by the importance weight. The map

estimate involves just picking the particle with the largest weight [8]. For the positioning system, the expected value is used.

A more detailed description of this algorithm and its implementation is beyond the scope this thesis and it will be given in a future thesis.

This chapter provided an overview of the four main parts: radio frequency reference system, dead reckoning system, digital mine map and algorithm for the positioning system. The next chapters covers the design and test of dead reckoning system hardware.

3. Hardware Design

Dead reckoning is a common method used to derive position on the basis of three distinct inputs: a set of starting coordinates, the direction of travel and the acceleration. The hardware design of a dead reckoning sensor system (DRSS) is the main focus of this chapter.
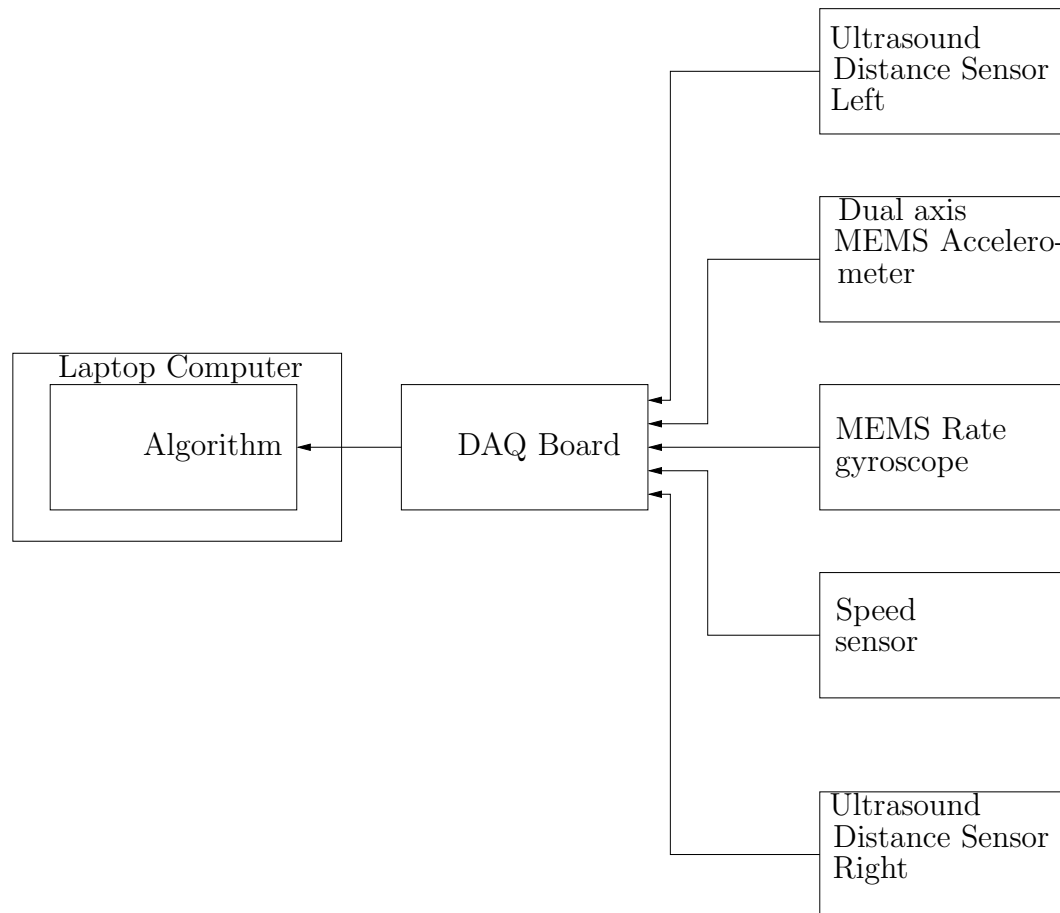

Figure 3.1: Dead reckoning sensor system for the mine positioning system

A block diagram of the proposed dead reckoning sensor system for use in the mine positioning prototype is given in Figure 3.1. As it is shown in this block diagram, the output of the ultrasound distance sensors is the measurement of the distance to the left wall, m_l and to the right wall m_r. The output of the dual axis MEMS (Micro Electro Mechanical System) accelerometer provides the measurement of the acceleration in the forward direction, a_f, and the acceleration in downward direction, a_d. The output of the MEMS rate gyroscope provides measurement of bearing rate, $\dot{\theta}$, and the direction of travel is measured by integrating $\dot{\theta}$ with time. Measured speed, s could be calculated from the OBDII data if available. All of these analog output signals from the sensors are sampled with an A/D converter built within a data acquisition (DAQ) board. A sensor fusion algorithm for the mine positioning system uses these sampled sensor output signals and data from digital mine maps and thus finds the position of a vehicle.

Although various sensors were considered for this dead reckoning system, only sensors which were finally used have been included in the discussion in this thesis. The next few sections discuss the design of individual sensors connected with the data acquisition system to build the dead reckoning system.

3.1 Accelerometer Sensor

One of the primary objectives for the dead reckoning system is to estimate the distance traveled by a vehicle. The distance can be estimated using various techniques. One possible method uses an encoder. Encoders can measure the rotational motion of the vehicle's wheel and thus knowing the wheel circumference will give the distance traveled. But for the DRS of in-mine positioning system, the sensors need to be such that they require minimum installation time, cost and effort. The DRS also needs to be a stand alone system. An encoder based system would not meet these critera

since encoder has to be installed on the wheel axel. Therefore accelerometer sensors are a better choice to serve this purpose. A dual axis MEMS accelerometer sensor is used to measure acceleration in the forward and downward directions, where the downward value is used to determine the pitch. Double integration of acceleration in the forward direction gives distance traveled.

MEMS inertial accelerometer sensors are small, low weight, have low power consumption, short start-up time, are relatively inexpensive, have high reliability, low maintenance and are compatible with operation in harsh environments [3]. But the use of inertial sensors can be problematic because of the accelerometer bias and scale factors. Also since a dual axis accelerometer is used for the measurements, there could be cross axis coupling.

The main purpose of this section is to describe the evaluation of the MEMS based accelerometer ADXL203 and to gain deeper understanding of its operation. Accelerometer measurements are obtained using a pendulum test setup that is designed to measure accelerometer bias, scale factor and cross-coupling by comparing with expected results. The test setup is described in section 3.1.2.

3.1.1 MEMS ADXL203 Accelerometer

"The Analog Devices' ADXL203 is a high accuracy, high stability, low cost, low power, complete dual axis accelerometer. The ADXL203 accelerometer sensor is a surface-micromachined polysilicon structure and it is built on top of a silicon wafer. The structure over the surface of the wafer is suspended by polysilicon springs and these springs provide a resistance against acceleration forces. Using a differential capacitor that consists of independent fixed plates and plates attached to the moving mass, the deflection of the structure is measured. 180° out-of-phase square waves drive the fixed plates. Acceleration deflects the moving mass and unbalances the

Figure 3.2: Functional Block Diagram of ADXL203. Taken from Analog Devices'
Spec Sheet [14].
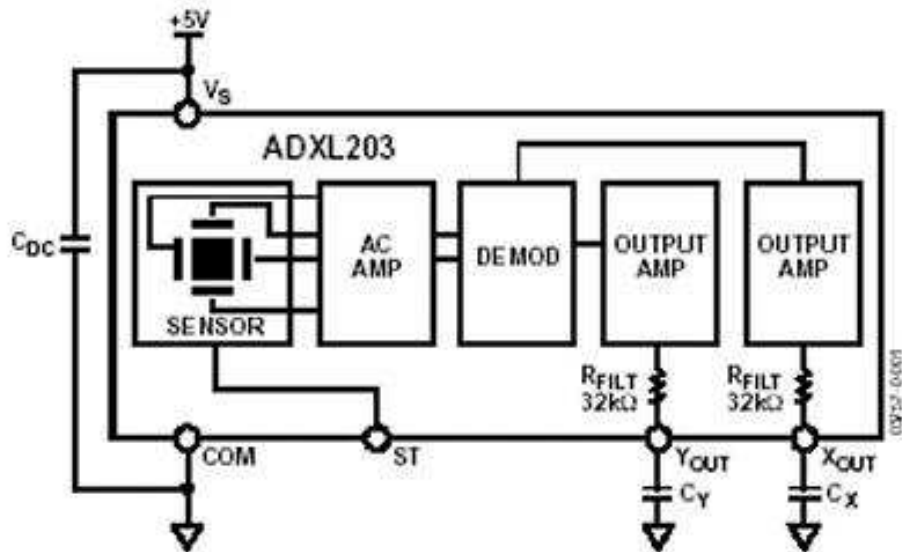
differential capacitor and this results in an output square wave whose amplitude is
proportional to acceleration. Phase-sensitive demodulation techniques are then used
to rectify the signal and determine the direction of the acceleration" [14].

The functional block diagram of the ADXL203 is given in Figure 3.2. The supply
voltage (V_s) for the sensor is 5 Volts. To have a constant supply voltage a capacitor
$C_{DC} = 0.1 \ \mu\text{F}$ is added in between the supply voltage, V_s and the common, COM.
Outputs of the demodulator are amplified and brought off-chip through two $R_{FILT} =$
32 kΩ resistors. The sensor outputs are Y_{out} and X_{out}.

The output signals, Y_{out} and X_{out}, of the accelerometer, which measure acceler-
ation in two directions are sampled by the DAQ board. The analog bandwidths of
the output signals have to be less than one half of the analog-to-digital sampling
frequency to avoid aliasing. The output of the ADXL203 has a typical bandwidth of
2.5 kHz. But here the ADXL203 is used to measure acceleration of a vehicle inside

mine tunnels and thus the required bandwidth is much lower. The ADXL203 has provisions for low pass filtering the Y_{out} and X_{out} pins. The signal bandwidths of Y_{out} and X_{out} can be set by changing capacitors C_Y and C_X shown in Figure 3.2. The equation for the 3 dB bandwidth for the output is

$$F_{3dB} = \frac{1}{2\pi(32k\Omega) \times C} \tag{3.1}$$

where C is the capacitor value.

Here 0.1 μF capacitors were chosen for both C_X and C_Y to give a 3 dB bandwidth of 50 Hz, which is well below the sampling frequency of 200 Hz meeting the antialiasing requirement. Another reason for selecting the 3 db bandwidth of 50 Hz is that it is below the power line frequency of 60 Hz, since frequency from high voltage cables in the mine is a significant problem. The tolerance of the resistor, R_{FILT}, varies by $\pm 25\%$ and so does the bandwidth.

An added benefit of the anti-aliasing filter, which reduces the analog bandwidth, is that it lowers the noise floor and thus improves the resolution of the accelerometer. The ADXL203 noise has the characteristics of white Gaussian noise, which contributes equally at all frequencies and has units of $\mu g/\sqrt{Hz}$. With the single pole roll-off characteristic, the typical noise of the ADXL203 is determined by rmsNoise=(110 $\mu g/\sqrt{Hz}$) $\times$ ($\sqrt{BW \times 1.6}$) [14]. With a 50 Hz bandwidth, the RMS (root mean square) noise is 0.98 mg.

The ADXL203 accelerometer has a number of important specifications. The zero g bias is the DC output level of the accelerometer when it is not in motion or being acted upon by the earth's gravity [15]. The technical specification for the ADXL203 states that it has high zero g bias accuracy. The output scale factor of an accelerometer indicates how many volts output are provided per g of applied acceleration [15] and the ADXL203 has a scale factor of 1000 mV/g [14]. The sensitivity accuracy is the

28

variation of the scale factor and the sensitivity accuracy of the ADXL203 is $\pm 4\%$ [14], thus the tolerance of the scale factor varies from 960 mV/g to 1040 mV/g [14]. The ADXL203 is designed in such a way that if the gravitational force is measured, for a supply voltage of 5 Volts, the expected output is 3.5 Volts for 1 g when there is no acceleration, 2.5 Volts being the zero g bias. Any deviation from the expected output will indicate bias offset. Similarly, when the accelerometer is not in motion, if the orientation of two axes is set in such a way that one accelerometer outputs exactly 1 g towards the downward direction, the other accelerometer should indicate 0 g acceleration towards horizontal or forward direction. Any offset from 0 g acceleration will indicate cross-coupling error. Since typically the two axes are aligned to within $0.1°$ and the internal alignment is constant, cross-coupling error is very small. This is apparent in the observed measurements and thus this term is not considered further. The accelerometer has a very typical non linearity of $\pm 0.2\%$ in its output. But presence of bias offset and unexpected scale factor might cause more error in the measurement and these are observed in the experimental pendulum test setup.

3.1.2   Pendulum Testbed

In Figure 3.3, the pendulum has a mass, m, hanging from an iron rod. When the pendulum is in motion, it has tangential acceleration, $a_t(t)$ and centripetal acceleration, $a_c(t)$, which are perpendicular vectors as shown in Figure 3.3. Theoretically, the angular acceleration, α, of a pendulum can be expressed as,

$$\alpha = \frac{d^2\rho(t)}{dt^2} = -\frac{g}{R}\sin(\rho(t)) - \frac{b}{m}\frac{d\rho(t)}{dt} \tag{3.2}$$

where $\rho(t)$ is the angular displacement with time, g is the gravitational acceleration, b is the damping constant and R is the length of the rod. For a small angle, $\sin(\rho(t)) \approx \rho(t)$ and the equation becomes

$$\frac{d^2\rho(t)}{dt^2} = -\frac{g}{R}\rho(t) - \frac{b}{m}\frac{d\rho(t)}{dt} \tag{3.3}$$

29
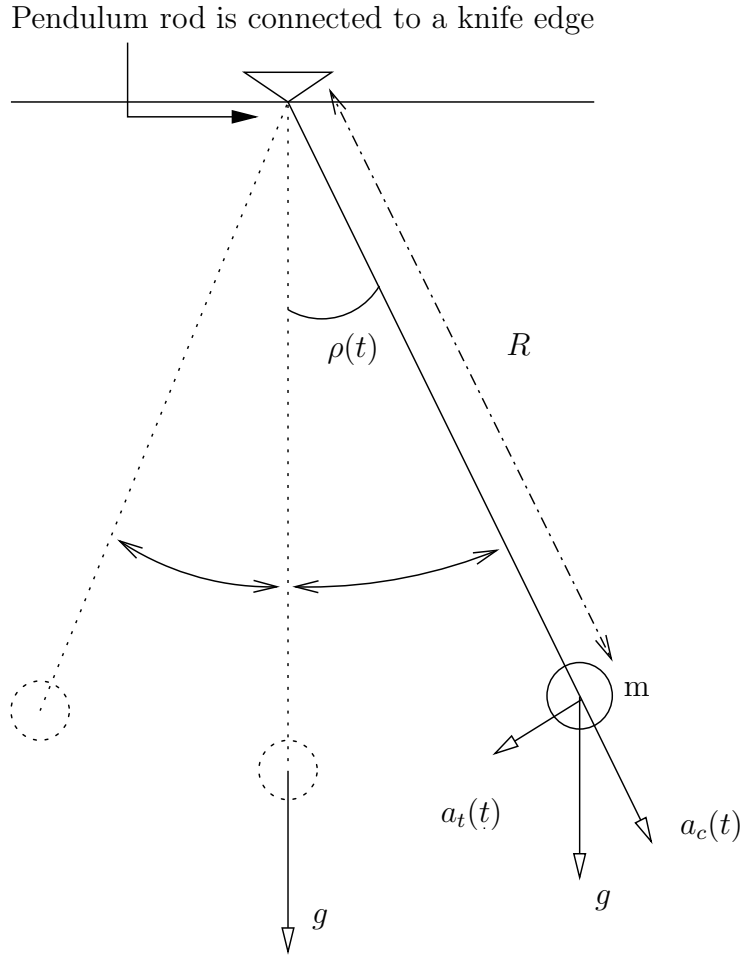
Figure 3.3: Model of pendulum test bed used to measure acceleration

Equation (3.3) is a second-order linear differential equation. To solve the equation, $\rho(t)$ needs to be a function such as $\rho(t) = e^{rt}$ (where r is a constant) so that its derivative is a constant multiple of itself: $\dot{\rho}(t) = re^{rt}$ and $\ddot{\rho}(t) = r^2 e^{rt}$. Substitution in equation (3.3) gives,

$$r^2 e^{rt} + \frac{b}{m} r e^{rt} + \frac{g}{R} e^{rt} = 0 \qquad (3.4)$$

$$\left(r^2 + \frac{b}{m} r + \frac{g}{R}\right) e^{rt} = 0 \qquad (3.5)$$

But e^{rt} is never 0. Thus, $\rho(t) = e^{rt}$ is a solution of equation (3.3) if r is a root of the equation

$$r^2 + \frac{b}{m}r + \frac{g}{R} = 0 \tag{3.6}$$

The root of this auxiliary equation (3.6) is

$$r = -\frac{b}{2m} \pm \sqrt{(\frac{b}{2m})^2 - \frac{g}{R}} \tag{3.7}$$

Solving the second order differential equation for $\rho(t)$ gives

$$\rho(t) = C_1 e^{(-\frac{b}{2m} + \sqrt{(\frac{b}{2m})^2 - \frac{g}{R}})t} + C_2 e^{(-\frac{b}{2m} - \sqrt{(\frac{b}{2m})^2 - \frac{g}{R}})t} \tag{3.8}$$

where C_1 and C_2 are constants and they depend on the initial displacement and the initial angular speed [16]. If we consider the initial displacement to be ρ_0, the initial angular speed $\frac{d\rho}{dt} = 0$ and damping constant $b = 0$, the equation becomes,

$$\rho(t) = \rho_0 \cos\left(\sqrt{\frac{g}{R}}t\right) \tag{3.9}$$

Using the expression for $\rho(t)$ in equation(3.2) tangential acceleration $a_t(t)$ and centripetal acceleration $a_c(t)$ can be calculated as

$$a_c(t) = g\cos(\rho(t)) \tag{3.10}$$

and

$$a_t(t) = -g\sin(\rho(t)) \tag{3.11}$$

Plots of calculated tangential acceleration a_t and centripetal acceleration a_c are shown in Figure 3.4. In these plots, acceleration is displayed as a function of g (gravitation acceleration). Note that the centripetal acceleration, a_c is twice the frequency of the tangential acceleration, a_t, every single time the pendulum mass swings from left to right and then right to left, the mass goes up and down twice.

Accelerometer biases and cross-axis couplings depend on the orientation of the accelerometer axis relative to the plane and internal angle among the axes. If the
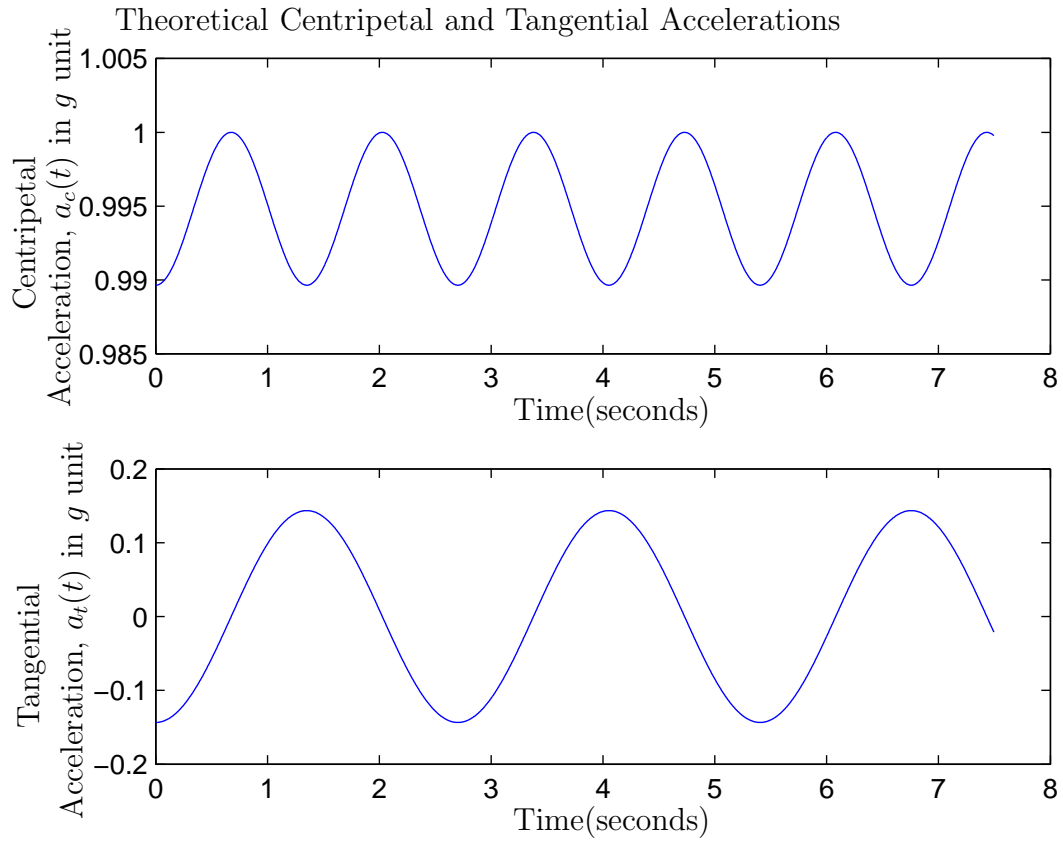
Figure 3.4: Theoretical centripetal and tangential accelerations of a pendulum

pendulum is not in motion and two axes are not perfectly horizontal or perpendicular to the earth's surface, there will be some bias offset. In addition, if these two axes are not perfectly perpendicular to each other there will be cross-coupling voltages on sensor outputs. The accelerometers are used to measure acceleration with respect to an inertial frame. The subject of interest is the translational acceleration for the positioning system which is typically less than 0.1 g. For all practical purpose gravity is the only other acceleration present.

By putting the pendulum in motion, the theoretical accelerations can be compared with the accelerations measured in this experiment and thus biases and scale factors

can be calculated.

A pendulum test setup, similar to Figure 3.3, was built to take the accelerometer measurements. A mass of 5.1 kg was suspended at the end of a 1.85 meter long iron rod. The mass of the rod was small enough to be be ignored and therefore, the centre of gravity was located at the suspended mass. The other end of the iron rod was connected with a knife edged iron bar parallel to the ground and that bar was suspended across two other knife edges to reduce damping friction. The dual axis MEMS accelerometer was mounted on the mass body with one axis directed towards the centre of the circular motion and the other axis directed toward the tangential direction.

3.1.3 Accelerometer Measurement Results

The pendulum testbed described in section 3.1.2 was used to evaluate the performance of the MEMS ADXL203 accelerometer. For a small initial angular displacement of $\rho_0 \approx 0.144$ radians, acceleration measurements were taken at a sampling rate of 200 Hz. An example of the measured accelerations is given in Figure 3.5 where it is apparent that the output is corrupted by noise. A low-pass FIR equiripple filter is used to remove the noise. Figure 3.6 shows filtered output of tangential acceleration measurement.

In Figure 3.7, plots of the theoretical and the measured tangential accelerations $a_{t_{theoretical}}(t)$ and $a_{t_{measured}}(t)$ are given. These plots indicate that the measured output for the tangential acceleration, $a_{t_{measured}}(t)$ has to be adjusted to compensate for the bias offset and scale factor. Here, the measured accelerations, $a_{measured}$ are related to theoretical accelerations, $a_{theoretical}$ by a simple model

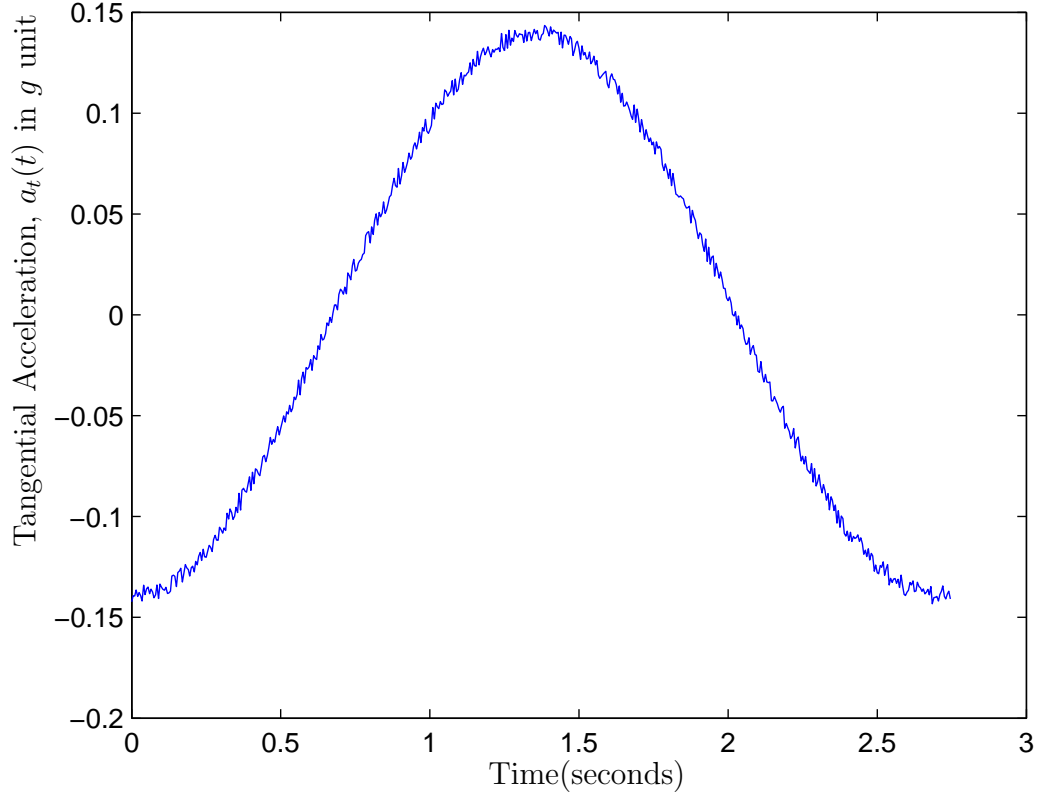$$a_{theoretical}(t) = a_{measured}(t)S + B \qquad (3.12)$$

33

Figure 3.5: Measured tangential acceleration. Showing that the output is corrupted by noise

where B is the bias and S is the scale factor.

In order to determine the bias offset and the scale factor, a polynomial curve fitting method is used to find the coefficients of a polynomial $P(a_{t_{measured}})$ of degree 1, $P(a_{t_{measured}}(t)) = P_1 a_{t_{measured}}(t)^1 + P_2$ where $P1$ and $P2$ represent scale factor and bias offset. Finding a best fit in a least squares sense attempts to minimize the sum of the squares of the ordinate differences (called residuals) between points generated by the function $P(a_{t_{measured}}(t))$ and corresponding points $a_{t_{theoretical}}(t)$ [17]. The coefficients $(P1, P2)$ of the polynomial are equivalent to bias (B) and scale factor
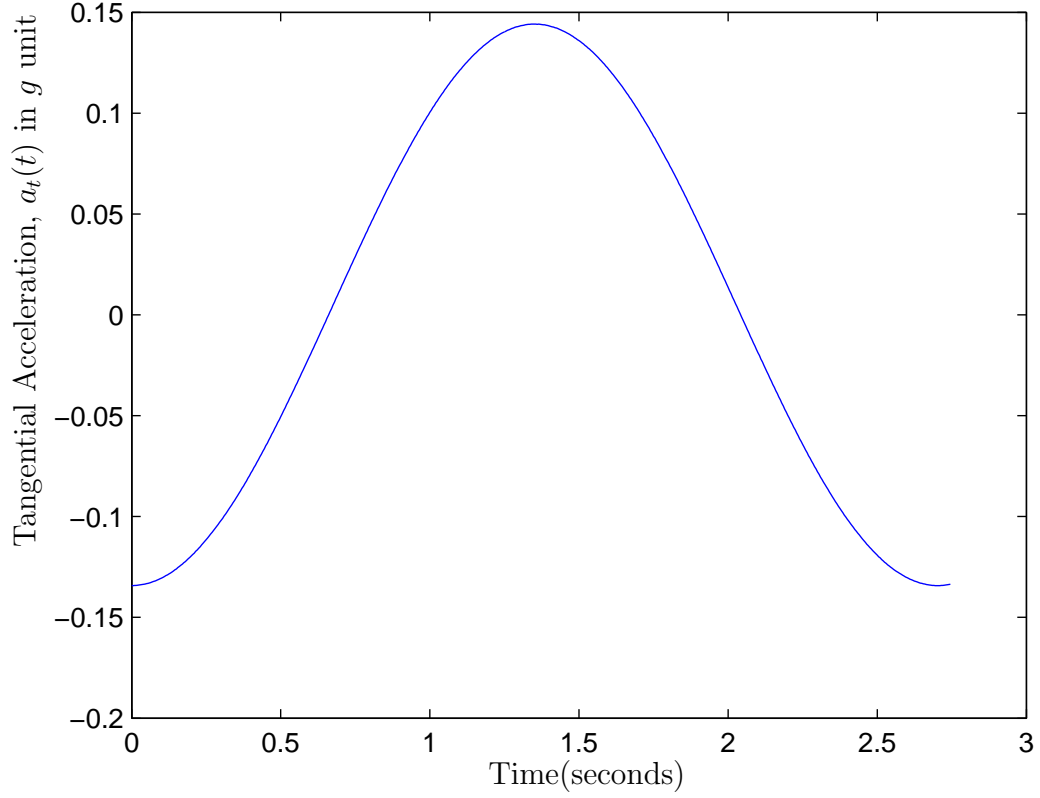
Figure 3.6: One cycle of a filtered tangential acceleration output

(S). Thus the relationships for the centripetal and tangential accelerations are

$$\hat{a}_{c_{theoretical}}(t) = P(a_{c_{measured}}(t)) = a_{c_{measured}}(t)S_c + B_c \qquad (3.13)$$

and

$$\hat{a}_{t_{theoretical}}(t) = P(a_{t_{measured}}(t)) = a_{t_{measured}}(t)S_t + B_t \qquad (3.14)$$

The biases for centripetal and tangential acceleration, B_c, B_t and the scale factors, S_c, S_t, are calculated for different cycles. An example of the fit is given in Figure 3.8 where the plot of the measured tangential acceleration, $a_{t_{measured}}$ fits with the expected theoretical acceleration, $\hat{a}_{t_{theoretical}}$ for a calculated scale factor, $S_t = 1.03$ and bias of

35
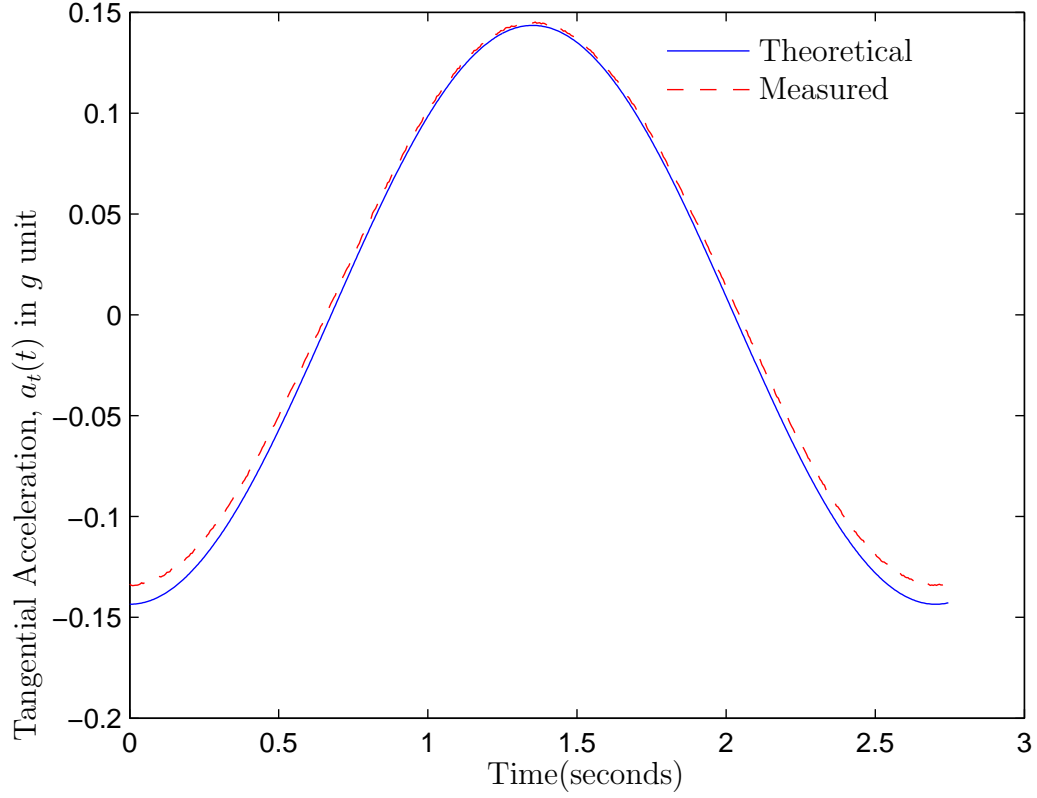
Figure 3.7: Comparison between theoretical tangential acceleration $a_{t_{theoretical}}$ (solid line) and measured tangential acceleration $a_{t_{measured}}$ (dashed line) tangential acceleration, before adjusting with scale factor and bias

$B_t = -0.005$. Similar approach is used to calculate scale factor, $S_c = 1.04$ and bias, $B_c = -0.01$ for centripetal acceleration.

There are some differences between data sheet and experimental values for scale factor and bias, but these are within the tolerance for the device. In ADXL203's specification sheet, it is mentioned that accelerometer's scale factor is typically 1 and it has a 0 g bias. But it is also mentioned on the specification sheet that the sensitivity may vary from 960 to 1040 mV/g. Figure 5 and 8 on ADXL203's specification sheet
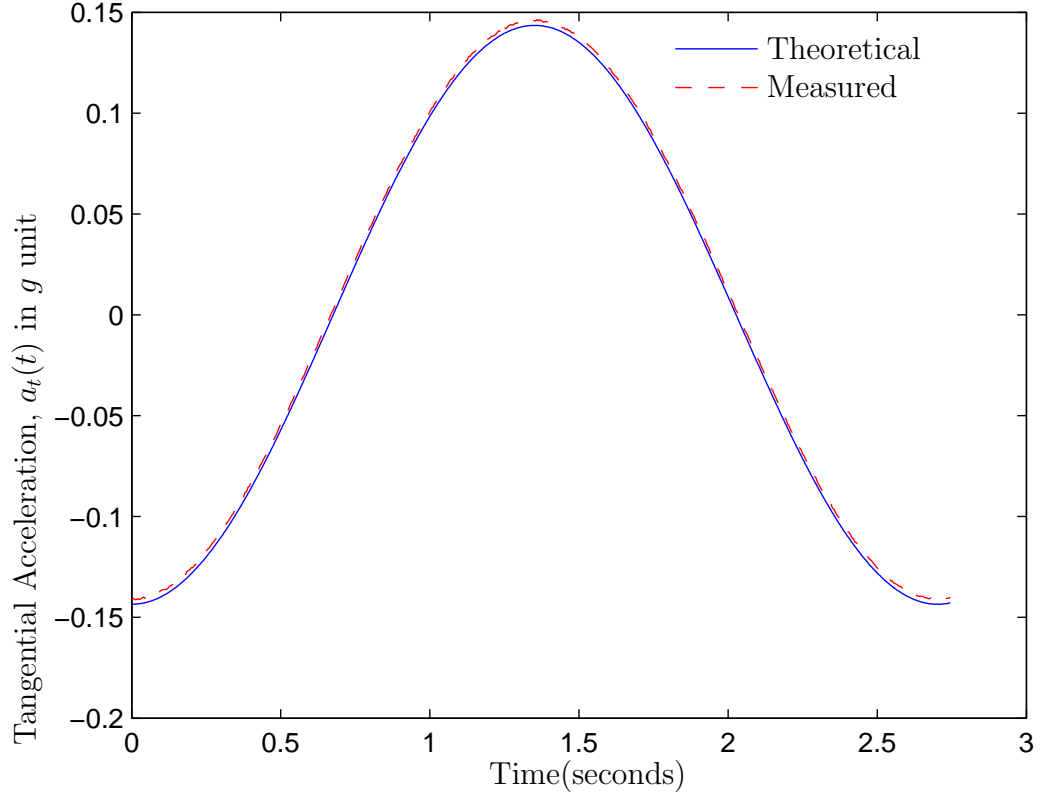
Figure 3.8: The first cycle of tangential acceleration, a_t after adjusting for scale factor 1.03 and bias -0.005 g . The solid line indicates theoretical acceleration, $\hat{a}_{t_{theoretical}}$ and the dashed line shows the measured acceleration, $a_{t_{measured}} S_t + B_t$

indicates that the 0 g bias may vary from -0.05 g to 0.08 g at ideal temperature of 25° Celsius [14].

The experimental test setup was designed to evaluate the bias and scale factor of a MEMS accelerometer. The results from experiments indicate that the biases and scale factors of accelerometers have to be adjusted.

3.2   Ultrasonic Distance Sensor

In the state variable model for the positioning system, two important observations are the distances from the vehicle to the two side walls of mine tunnel. Although there are various ways to measure the distance, ultrasonic sensors were chosen considering the requirements of proximity range of approximately 10 meter, the dusty environmental condition inside the mines, and the cost. There are a variety of ultrasonic transducers, such as piezoelectric, and electrostatic. The SensComp's series 600 environment grade electrostatic ultrasound transducer was chosen since it has a fairly low cost. Unit cost for transducer was $27. [18].

3.2.1   Operation of the Ultrasonic Sensor

SensComp's electrostatic transducer is similar to an electrical capacitor, with one fixed plate and one movable plate. The fixed plate is an aluminum disk with concentric groves on one side. The movable plate is a film of Kapton material coated on one side with a thin layer of Gold, which is stretched over the Aluminum backplate. The Kapton material acts as an insulator between the Gold and Aluminum. When an electrical potential of a certain frequency is placed between the two plates, the foil is attracted to the backplate. The moving foil displaces air and generates a burst of ultrasonic sound. The advantages of electrostatic technology are an ultra sensitive, responsive transducer with low ring characteristics. This desirable trait is well suited for detecting soft objects and ranging to targets at both near and far distances [18].

SensComp's series 600 Environment Grade transducer is specially intended for operations in harsh conditions at ultrasonic frequencies. The frequency of ultrasound is 50 kHz. This transducer has a beam angle [18] of 15°, as shown in Figure 3.9, and the distance range is from 0.15 meter to 10.7 meter. It has a resolution of ±1% over the entire distance range. This transducer and other supporting electronics are
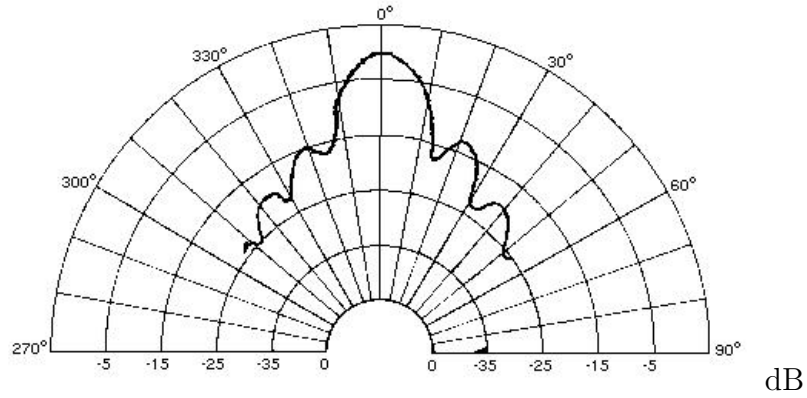
Figure 3.9: Beam pattern for the ultrasound transducer [18]

integrated in SensComp's 600 series smart sensor. The analog output of the sensor, which is proportional to the distance, has a range of 0-5 Volts with a repetition rate of 5 Hz.

The operational signals for the SensComp's series 600 Environment Grade sensor are shown in Figure 3.10. After applying power (VCC) a minimum of 5 ms must elapse before the input signal (INIT) is initialized by making it high. All internal circuitry is reset and the oscillator stabilizes during this period. When INIT is taken high, drive to the transducer (XDCR) output occurs. Sixteen pulses at 49.4 kHz with 400 Volts amplitude will excite the transducer and at the end of the sixteen pulses, a dc bias of 200 Volts will remain on the transducer as recommended for optimum operation. In order to make sure that the DC voltage power source can maintain 2 Amperes when the transmit drive to the transducer occurs [18], a 1000 μF electrolyte capacitor is used in between the ground and power source. Then all that is left is to wait for the echo signal (ECHO) of the transmitted signal reflected from an object. The transmitted and reflected sound travel at approximately 2.95 millisecond/meter. The returning signal, ECHO, is amplified and appears as logic high. The time difference between INIT going high and the ECHO going high, $\triangle t$, is proportional to the distance of
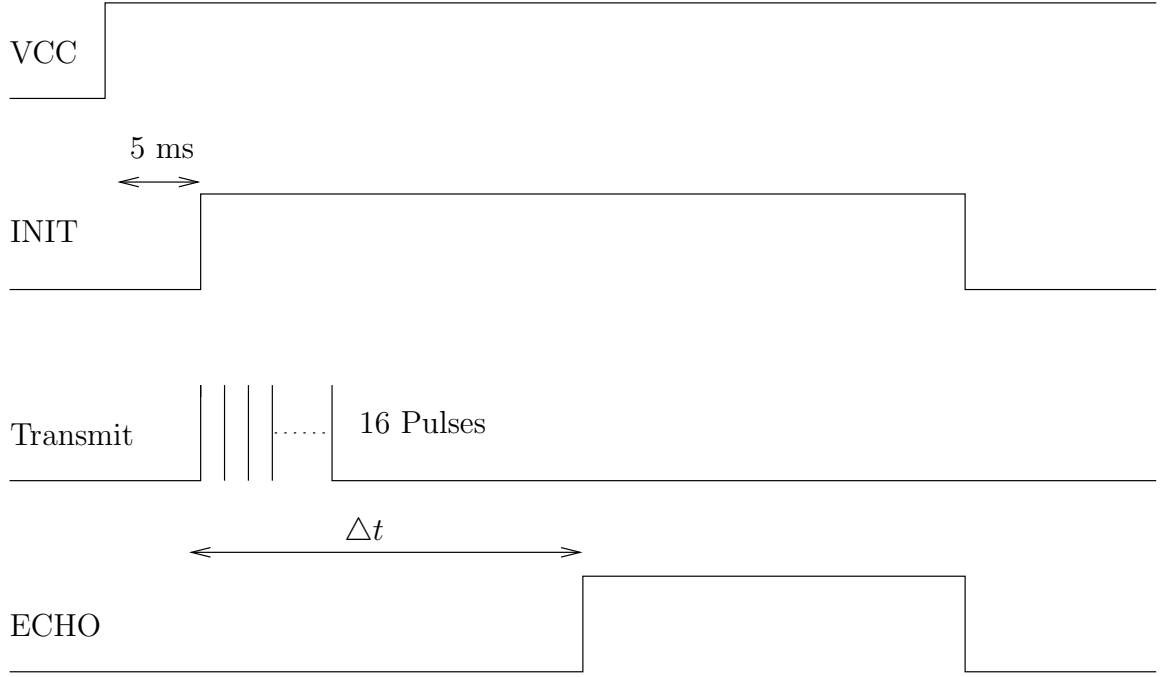
39

Figure 3.10: Operation of Ultrasonic Sensor [18].

the target from the transducer. The amplitude of the analog output voltage of the sensor is proportional to $\triangle t$ or the distance of the target. The cycle is repeated at 5 Hz by returning INIT to a low-logic level and then raising it high. The sensor's output is calibrated in such a way that any object located closer than the minimum distance range ($\triangle t$ is smaller than the minimum detectable time difference) will cause an output of 0 Volts and any object located further from the maximum distance range will cause an output of 5 Volts. The output voltage will be linear proportional to distance in between the maximum and the minimum of the range.

3.2.2 Evaluation of the Ultrasound Sensor

Since the positioning algorithm uses the distance from the side walls of mine tunnels as observations in locating an object inside an underground mine, the accuracy

of the measured distance is important. Therefore, it is important to evaluate the operation of this sensor and gain knowledge about the presence of errors associated with its measurements. This was done using a simple test bed developed to measure the accuracy of the sensor and how fast the sensor can respond to the change in distance.
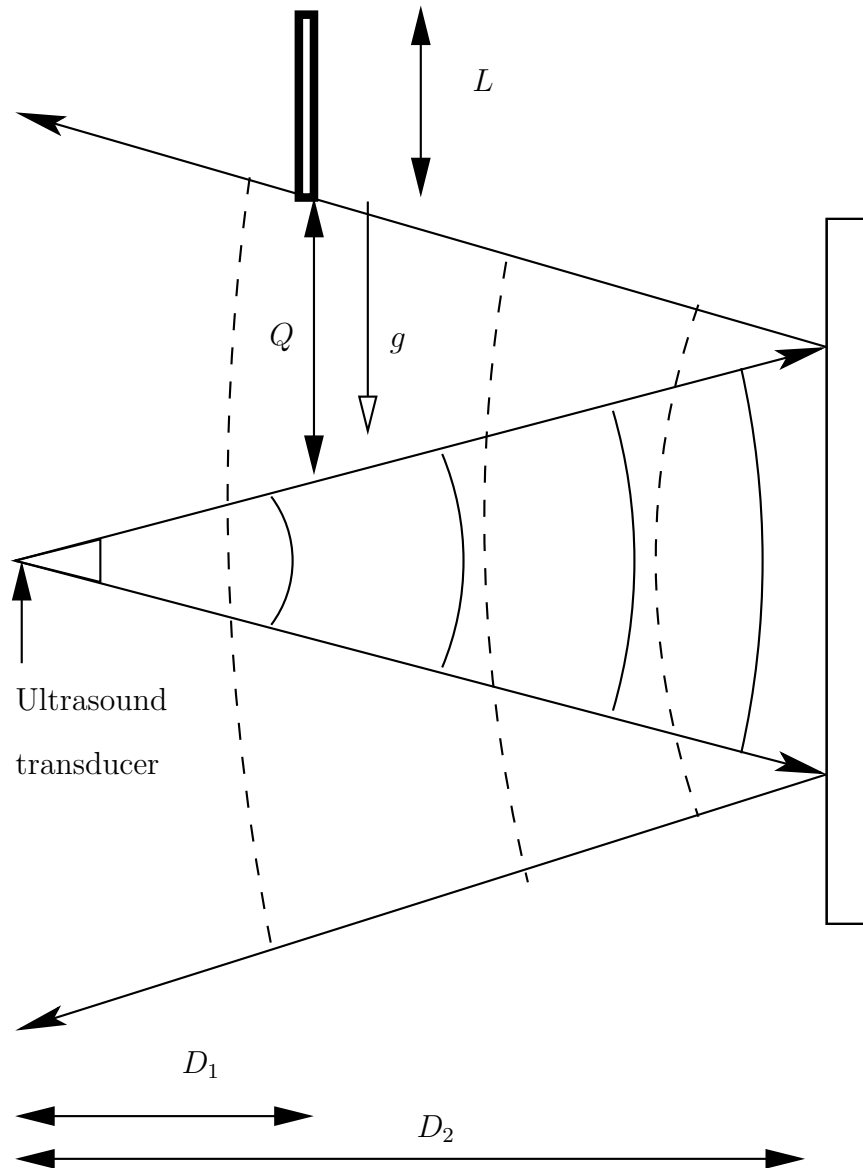

Figure 3.11: Ultrasound transducer testbed before dropping the object
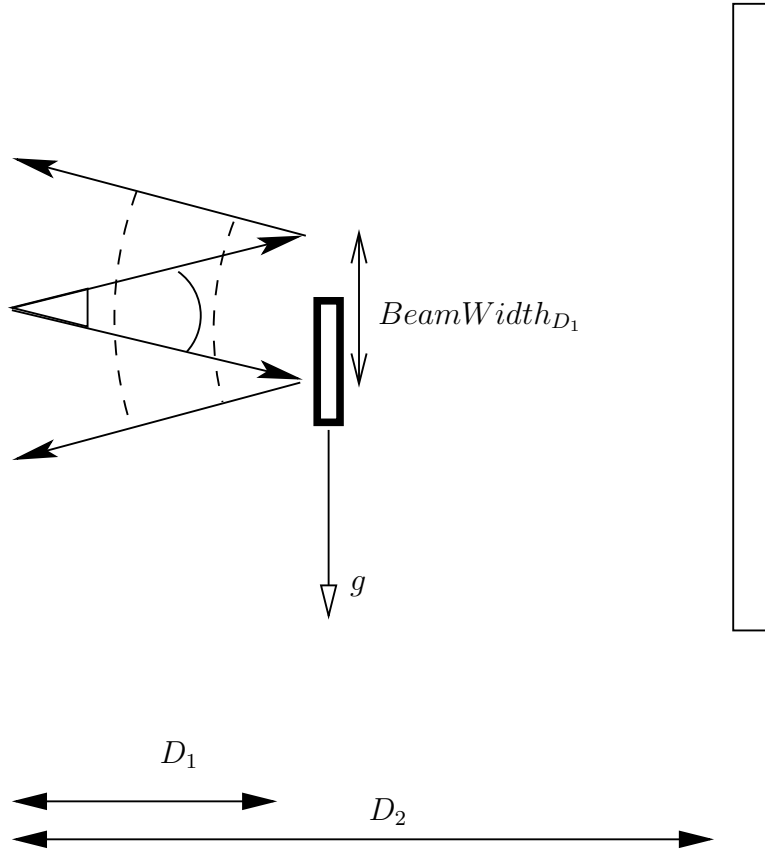
Figure 3.12: Ultrasound transducer testbed after the object is dropped

A simple test, as shown in Figure 3.11, was set up, where an object of length L is dropped in between the distance sensor and a wall located D_2 meters from the transducer. The length of the object, L, is such that it is detectable by the sensor for more than 0.2 seconds. It is dropped a distance of D_1 meters from the sensor. The object has a gravitational acceleration of g. It is assumed that the object is only observed by the distance sensor when it crosses $\pm 15°$ from the middle of the beam at D_1. The beamwidth at that point is $BeamWidth_{D_1} = 2\tan(15°)D_1$. When the object is dropped as shown in Figure 3.12, the time difference between when the object first enters the beam after falling for a distance of Q meters and when the very last part of the object leaves the beam after crossing the entire length $Q + L + BeamWidth_{D_1}$

10 m/5 volt
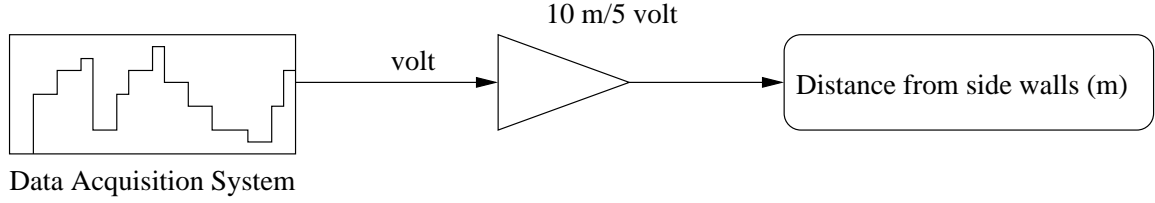
volt

Distance from side walls (m)

Data Acquisition System

Figure 3.13: Measuring distances from side walls by ultrasound sensors

is $\triangle t$. $\triangle t$ has to be greater than 0.2 second since the repitition rate of the sensor is 5 Hz.

In this test, the distances are $D_1 = 2$ m, $D_2 = 8$ m and the length of the object is $L = 0.2$ m. The distance, $Q \approx 0$ m. Therefore the sensor will have 0.51 second to detect the object. The experiment has been kept simple to observe the response time. The output from the sensor is sampled with the data acquisition board as shown in Figure 3.13 using a sampling frequency of 100 Hz. The sampled output voltage is multiplied by a factor of 2 meter/Volt to convert the voltage to meters.

The result from the test is shown in the plot in Figure 3.14. The plot clearly indicates that the response time of the sensor was adequate to distinguish the object from the wall. The sensor could measure the distance from the non-moving wall with an error less than 10 cm. Typically a tunnel opening has a width of 10 meter and a GPR carrying vehicle travels at a speed less than at 20 KMH. Therefore the expected response time to recognize an opening is 1.8 second which is more than 0.51 second. The purpose of this experiment was not only to evaluate the transducer's operation in measuring distance adequately, but also to show that the response time is sufficient to recognize openings (typically tunnel width is 10 meter) in mine tunnels.
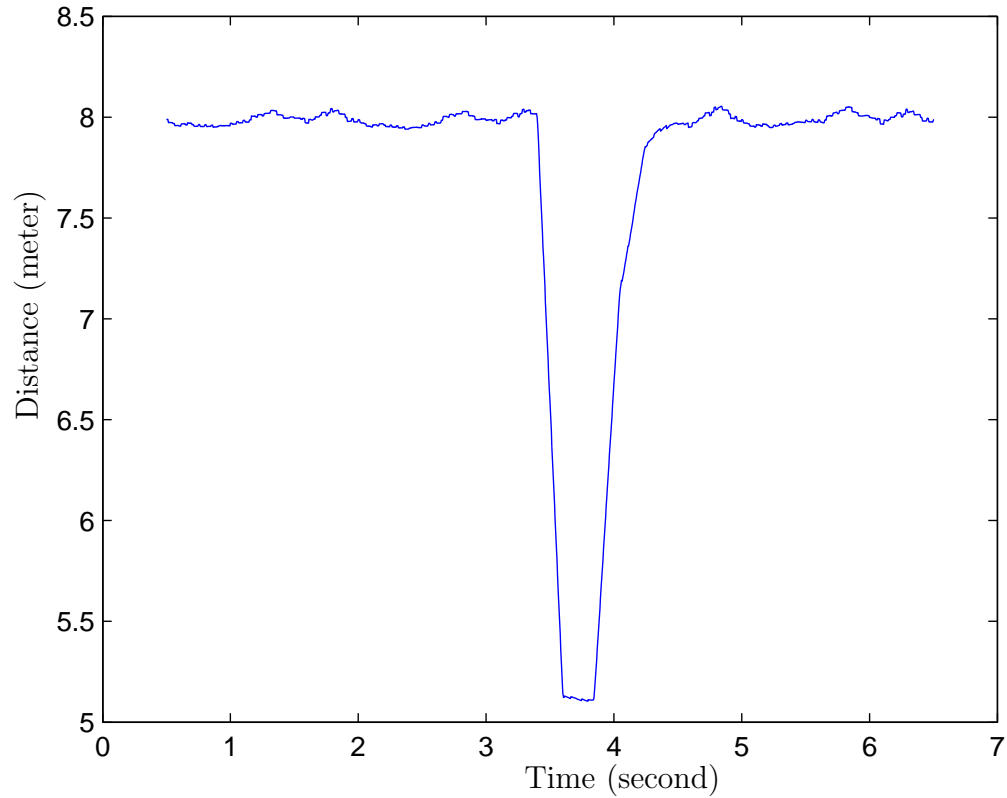
Figure 3.14: Distance measurement test of an ultrasonic sensor

3.3   Gyroscope

The positioning algorithm needs the direction of travel and this will be measured using a gyroscope. There are two kinds of gyroscopes. The first kind is called a displacement gyroscope and it is used to measure the angle of a vehicle's turn about some defined axis [3]. The second kind is called a rate gyroscope and it is used to measure angular rate of turn about some defined axis [3]. In order to build the dead reckoning system for in-mine positioning system, the latter kind was chosen.

3.3.1 Rate Gyroscope

Rate gyroscopes are used to measure angular rate, which is equivalent to measuring how quickly an object is turning. MEMS rate gyroscopes are non-rotating devices that use the Coriolis acceleration effect [A.1] on a resonating proof mass to detect inertial angular rotation. Therefore, this sensor relies on the detection of the force acting on a mass that is subject to linear vibratory motion in a frame of reference which is rotating about an axis perpendicular to the axis of linear vibratory motion. The Coriolis force acts in a direction that is perpendicular to both the axis of vibration and the axis about which the rotation is applied, as shown in Figure 3.15.

Rotation

Linear Vibratory Motion
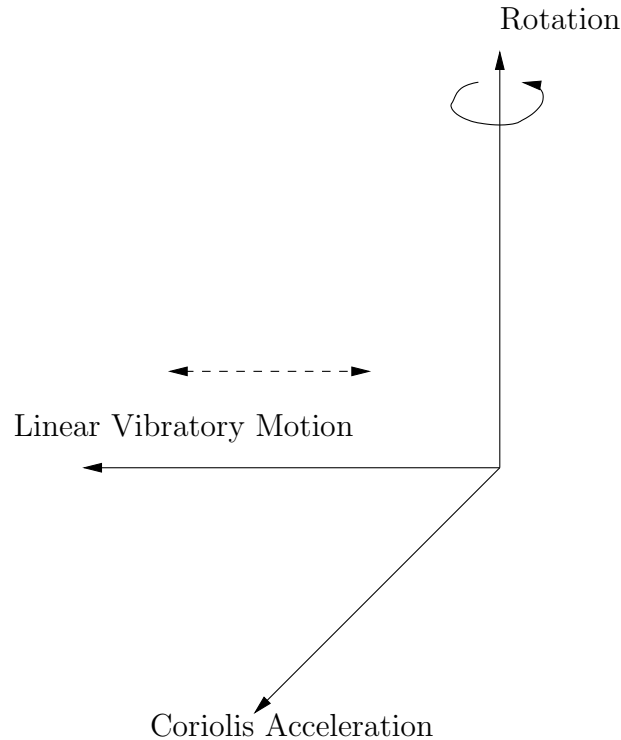
Coriolis Acceleration

Figure 3.15: Generation of coriolis acceleration

The attached mass can vibrate only in one direction. In Figure 3.16, it is shown that when the resonating mass moves toward the outer edge of the rotation, it is

accelerated to the right and exerts a reaction force to the left on the frame due to coriolis force. When the mass moves toward the centre of the rotation, it exerts a force to the right, as indicated by the arrow. In order to measure the Coriolis
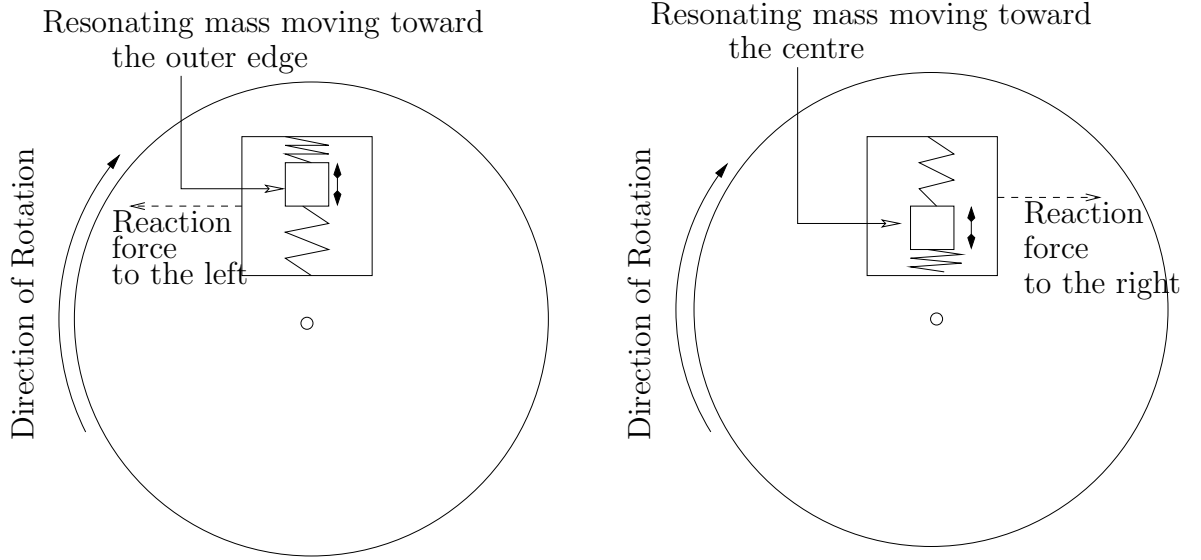
Figure 3.16: Acceleration effect in response to a resonating mass suspended inside a frame [19].

acceleration, the frame containing the resonating mass is attached to the substrate by springs at 90° relative to the resonating motion and Coriolis sense fingers are used to capacitively sense displacement of the frame in response to the force exerted by the mass, as shown in Figure 3.17 [19].

In a MEMS rate gyroscope, the rotation is typically measured in reference to yaw axis as in Figure 3.18. But the gyroscope can be mounted on its side so that the yaw axis can become the roll or pitch axis.

For the mine positioning system, an Analog Devices ADXRS150 rate gyroscope is used. The ADXRS150 operates on the principle of the resonator gyro. The functional block diagram of the ADXRS150 is given in Figure 3.19. There are 20 pins indicated
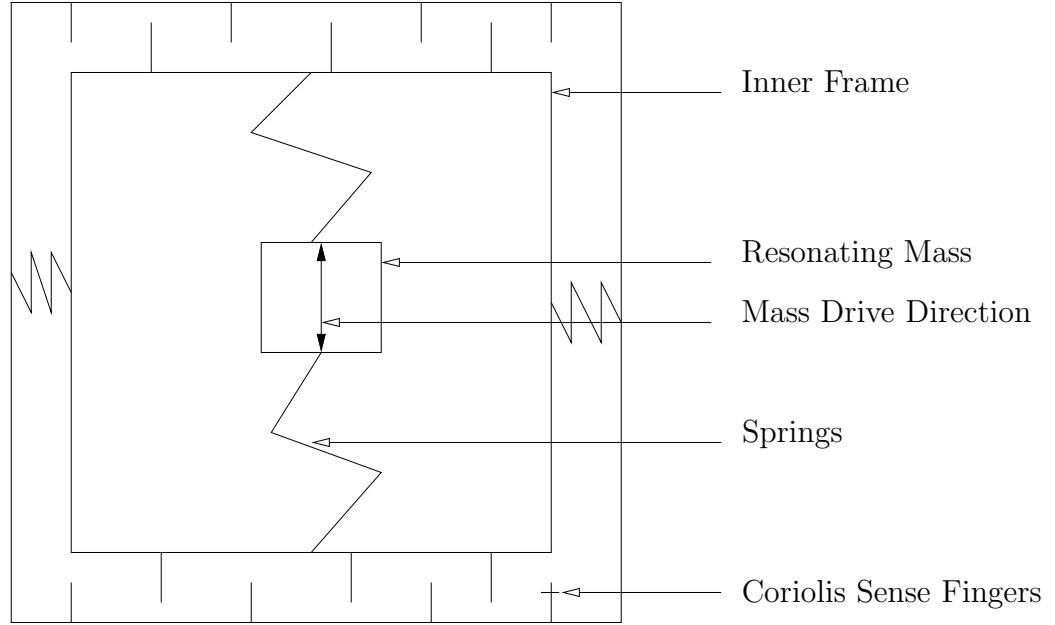
Figure 3.17: Schematic of the gyro's mechanical structure [19].
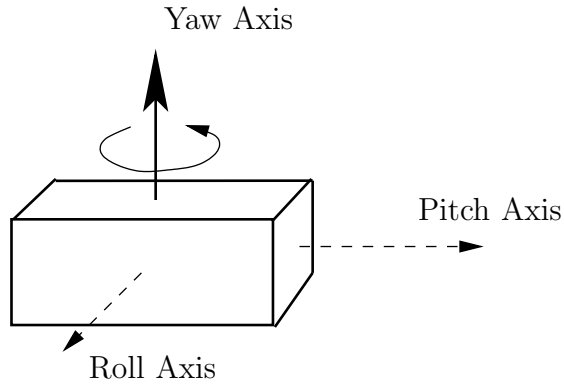
Figure 3.18: Gyro turning in respect to Yaw axis

by the circles in the figure. A 5 Volt power supply is connected to pin $AVCC$ (3A) and the pin $AGND$ (2G) is connected to ground. "The electrostatic resonator in the ADXRS150 requires between 14 V to 16 V for operation. Since only 5 Volts is typically available in most applications, a charge pump is included on-chip. If an external 14 V to 16 V supply is available, the two capacitors on CP1 and CP4 can be

omitted and this supply can be connected to CP5 (Pin 7D) with a 100 nF decoupling capacitor in place of the 47 nF." [20] The sensor output is fed to a series of gain
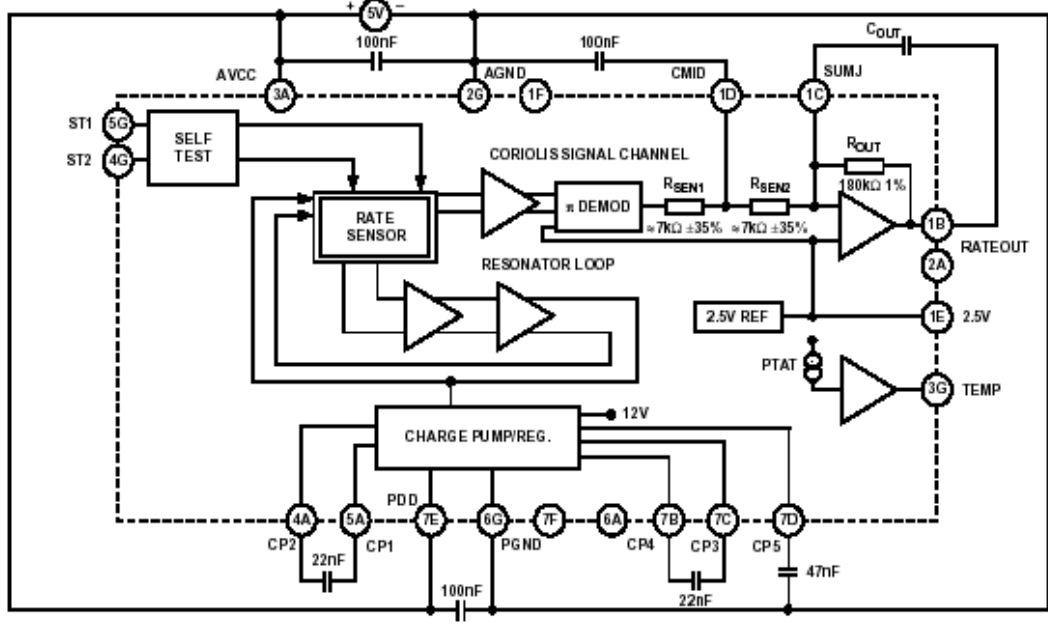
Figure 3.19: Functional Block Diagram of ADXRS150. Taken from Analog Devices' Spec Sheet [20].

and demodulation stages that produce the electrical rate signal output at the pin $RATEOUT$ (1B, 2A). An antialiasing filter is used to limit the bandwidth to 40 Hz. External capacitors $CMID$ and C_{OUT} can be used in combination with on-chip resistors to create two low-pass filters to limit the bandwidth of the ADXRS150's rate response. The 3 dB frequency, set by R_{OUT} and C_{OUT}, is

$$f_{OUT} = \frac{1}{2\pi R_{OUT} C_{OUT}} \tag{3.15}$$

In this case R_{OUT} and C_{OUT} are set to 180 kΩ and 22 nF, respectively to give bandwidth of 40 Hz. The ADXRS150 rate gyro has a range of $\pm 150°/s$ and sensitivity

48

of $12.5mV/°/s$. The rate gyroscope has a typical nominal output voltage of 2.5 V. The difference between the nominal voltage and the output voltage at $RATEOUT$ is proportional to the rate of turning angle. The dual-sensor design rejects external g-forces and vibration. Evaluation of the ADXRS150 was done before integrating it with the overall positioning system.

3.3.2 Gyroscope Evaluation

The gyroscope test setup is shown in Figure 3.20. The gyro sensor is placed on the top of a flat circular moveable disc and the disc is turned manually clockwise and anticlockwise. After measuring the output voltage from the Gyro sensor, the nominal voltage is subtracted and resultant voltage is divided by the sensitivity ($12.5mV/°/s$) to transform it to $°/s$ units. Later the output from gain block, shown in Figure 3.21, is integrated over time to measure the total change of angle. In this evaluation test, the rate of change was not kept constant and it is an important issue since when a vehicle will make turn inside mine tunnels, it is unlikely the turn will occur at a constant rate. Therefore emphasis was given to the total change of angle.

From a start point of 0°, the disc was turned to a particular angle and data for rate of change in angle was logged into the computer. After each measurement, the disk was turned back to 0°. The process was applied to measure turning angles of 30°, 60°, 90°, 120°, 150°, 180°, −30°, −60°, −90°, −120°, −150° and −180°. Later the logged data was integrated as described above and compared with expected result. Three measurements were taken for each case and the average of these three measured values were compared with expected angle. Table 3.1 compares the expected change of angles with the measured data. Standard deviation of three measured values for each turning angles are also given.

The results shown in the Table 3.1 indicate how close the measurement is to the

49
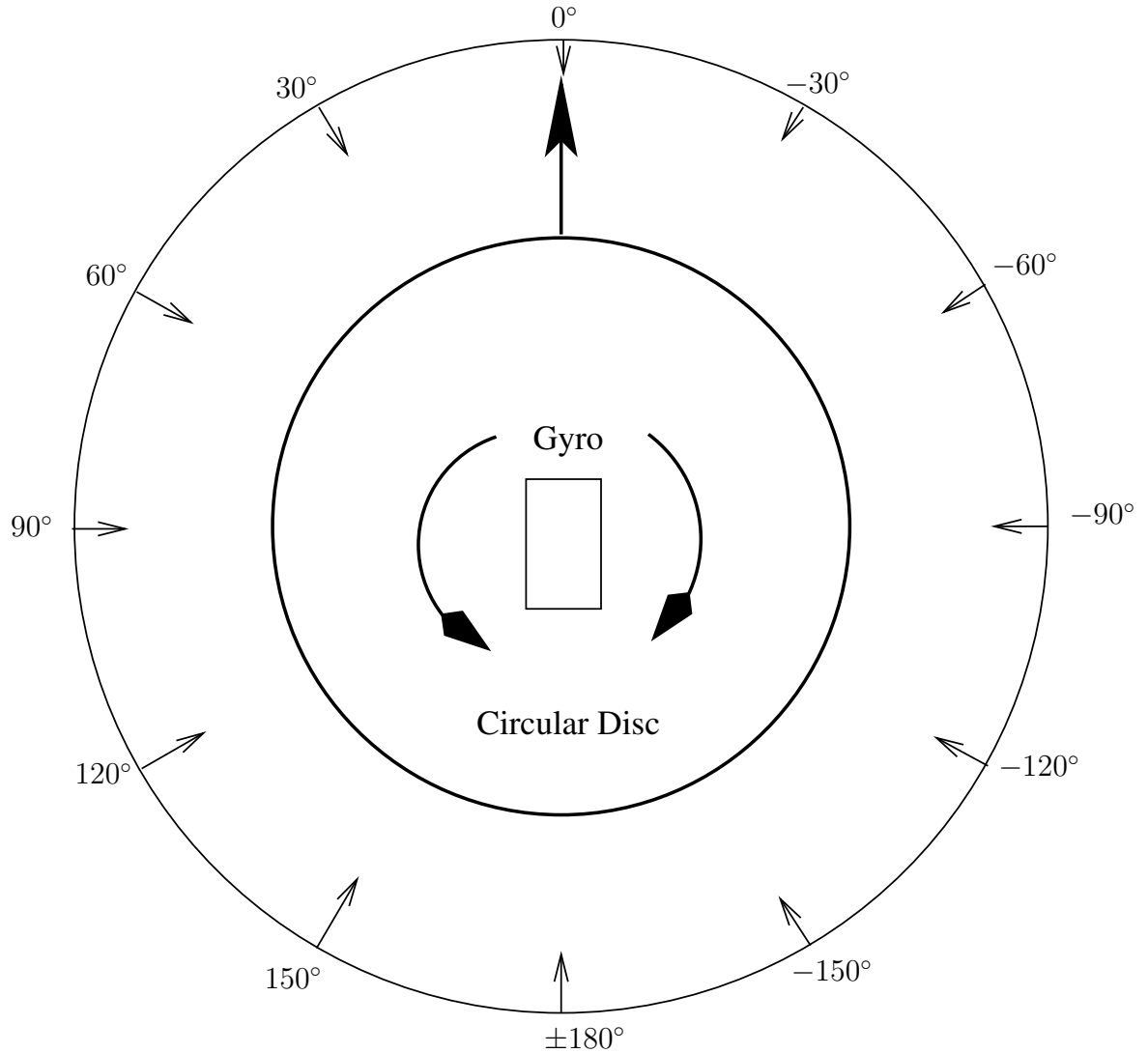
Figure 3.20: Rate Gyroscope test bed

expected value. It is observed that the measured angles were closer to the expected angle value for smaller turns than larger turns and negative angles had less error than positive angles. Average error in turning angle is 1.43%. The differences between the expected and measured value could be caused by the bias and scale factor of the gyroscope. Another explanation could be the difference between expected and measured nominal voltage. As the Analog Devices' specification sheet states that
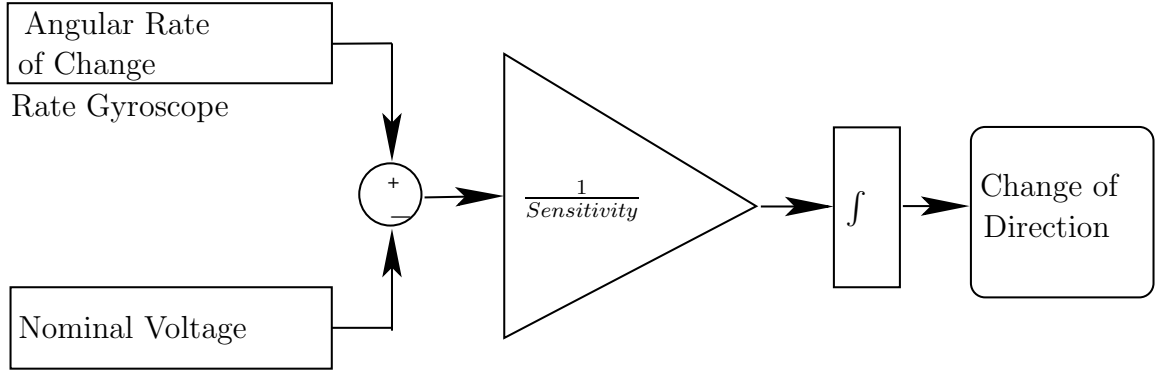
Figure 3.21: Block diagram for rate gyroscope test setup

Table 3.1: Rate gyro test setup measurements

Expected Angle (°)	Avg Measured Angle (°)	Difference(°)	StdDev
-180	-181.33	1.33	2.25
-150	-151.24	1.24	1.39
-120	-121.24	1.24	1.07
-90	-89.91	0.08	0.81
-60	-59.41	0.58	0.10
-30	-29.07	0.93	0.04
30	30.17	0.17	0.06
60	60.41	0.41	0.11
90	91.96	1.96	0.65
120	122.14	2.14	2.13
150	153.28	3.28	2.34
180	184.14	4.14	2.84

when there is no turn occurring, the typical nominal voltage for an analog supply voltage of $AVCC = 5$ V is $AVCC/2 = 2.5$ V. But it was found from the measurement

that for that particular gyroscope in use, the nominal voltage was approximately 2.34 V. Though the adjustment was made in the integration calculation, this might have still caused some error. Again the nominal voltage drifts with time and every time the gyroscope is powered up. It was found that the gyroscope required a warming up period of few minutes before the nominal voltage stabilizes. But since this error range may vary from one gyroscope to another gyroscope, calculating the bias and scale factors was avoided. Moreover the idea behind the test was to gain knowledge about the operation of the gyroscope.

3.4   Speed Sensor

A speed sensor could provide additional information for the positioning system, such as the initial speed, though this can be calculated from the time difference when the Radio Frequency receiver mounted on the vehicle passes two consecutive Radio Frequency reference beacons.

Potential speed sensors could be mounted on the different parts of a vehicle. Considering the dusty conditions, optical speed sensors should be avoided. Focus can be given to inductive speed sensors. An inductive engine speed sensor is mounted on the vehicles crankshaft and is usually where the speedometer gets its data, whereas wheel speed sensors are located individually at each wheel or axle generating a signal that changes with wheel speed. The sensor functions on the principle of magnetic induction. In this case, the sensor consists of a magnet mounted in close proximity to a ring that spins at wheel speed causing a sine wave (a low-voltage rhythmic pulse) to be generated by the magnet. A computer reads this signal as wheel speed. But a requirement of the positioning system is that it should be easily mountable on a mine vehicle. Thus a connection to an board diagnostic system such as OBDII is more convenient. OBDII is available for vehicles made after 1996 [6]. OBDII data

contains various information about a vehicle including information that can be used to calculate speed of the vehicle.

3.5 Data Acquisition

In the previous sections, various sensors were discussed and their evaluations were presented. The output signals from all of these sensors are sampled and logged to a laptop computer through data acquisition system. A National Instrument data acquisition board DAQCard-AI-16XE-50 is used in this case. The DAQCard-AI-16XE-50 is an I/O board with 16 single or 8 differential analog input channels (16-bit) with a maximum sample rate of 200 kSymbols/sec, 8 digital input and output lines, and 2 counter/timers (24-bit) with a maximum source clock rate of 20 MHz [21].

Signals from the sensors will be corrupted by noise. The typical sources of noise are thermal noise, shot noise and noise from variations in the supply voltage, and variation in the reference voltage. The noise power from these sources can vary and they can be reduced using bypass capacitors before conversion. Noise can also be produced due to quantization error while data conversion. However, A/D converters will always have quantization noise and the process of A/D conversion is limited by resolution and quantization noise. For the dead reckoning system used here, output range for each sensor is 0-5 Volts. Therefore a 16 bit A/D will have 2^{16} steps and a resolution of 5 Volts/2^{16} step=0.076 mV/step. There will be $\pm 1/2$ LSB (0.038 mV) error associated with quantized data.

There are many ways to lessen errors in the A/D converted data. One technique would be to simply just increasing the number of bits at the A/D converter. Increasing the number of bits will also increase the cost associated with the conversion. Another technique would be to dynamically change the signal's output range. For an example,

a vehicle inside mine tunnel will never travel at a acceleration of g and in fact it will be much less than that. Therefore the output range of 0-5 V can be changed to more practical range of minimum 2 V to maximum 3 V when 2.5 V is the nominal voltage. Thus the same number of bit (16 bits) can be used to convert a signal of 1 V range rather than of 5 V range. A description of how the range can be changed by adjusting scale factor and offset, can be found on the article by Kitchin [15]. In order to do so, the circuitry of the sensor needs to be modified. Another way to improve the resolution is by oversampling and subsequent discrete time filtering and downsampling. This technique allows an increase in step size of the quantizer or, equivalently, a reduction in the number of bits required in the A/D conversion and this is the technique that is used for this prototype. Although the future mine positioning system might use an A/D converter with higher resolution or a sensor with lower dynamic range, oversampling and subsequent discrete time filtering and downsampling is only considered in this thesis. A detail description of the theory behind this technique can be found in Oppenheim [22] and Staller [23].

3.5.1 Implementation of the Data Acquisition System

The signal-to-quantization noise ratio (SQNR) in decibels can be expressed as

$$SQNR = 6.02B + 1.76 + 10 \log_{10} \left[f_s/(2W) \right] \tag{3.16}$$

where B is the number of bits, f_s is the sampling frequency, and W is the signal bandwidth. If f_s is oversampled by M times, $SQNR = 6.02B + 1.76 + 10 \log_{10}(M)$ [24]. Therefore, the SQNR can be increased by oversampling the analog signal. The oversampling technique increases SQNR by spreading out the quantization noise across wider frequency band. Equation 3.16 shows that the quantization noise power is reduced by a factor of $10 \log_{10}(M)$dB. For example, if the sampling frequency is oversampled by $M = 4$, the quantization noise is reduced by 6dB, which is equivalent to

an increase of 1-bit resolution.

The bandwidth of all of the sensor signals is 50 Hz or less. Anti-aliasing filters, which were discussed for each of the sensors, are used to limit the bandwidth. In total there are five analog signals to sample through the same A/D converter and the minimum sampling rate is 100 Hz per channel. This is much less than the allowable sampling rate of 200 kSymbols/sec permitted for the A/D converter. In order to improve the resolution by 1 bit, the signals need to be oversampled by factor of 4, which is equivalent to 400 Hz, according to Staller [23]. Although the sampling rate could have been increased more than 400 Hz to further increase the accuracy of the data, it has been avoided since this is just a prototype of the positioning system. Computation time needed for post processing by the algorithm is also considered.

The data acquisition uses MATLAB's data acquisition toolbox. The MATLAB data acquisition toolbox provides a complete set of tools for analog input, analog output, and digital I/O for a variety of PC-compatible data acquisition hardware. The toolbox can configure external hardware devices such as the DAQCard-AI-16XE-50 to read data into MATLAB for immediate analysis. MATLAB Code used in this case is as follows. Five channels were used to sample signals from 5 sensor outputs at a sampling rate of 400 Hz. The sampled data was logged into files for post processing.

```
%Creating an analog input object to support a National Instrument's
%DAQ card
ai = analoginput('nidaq',1);
%Adding 5 channels to analog input object
ai_channels = addchannel(ai,0:4);
%Setting up sampling rate to 100 Hz for 5 analog input channels
set(ai,'SampleRate',400);
```

```
%Varifying the actual sampling rate that is set

ActualRate = get(ai,'SampleRate')

%Setting up input voltage range to 0-5 Volts

ActualRange = setverify(ai.Channel,'InputRange',[0 5]);

%Setting up the number of samples to aquire to infinity after the

%trigger occurs

set(ai,'SamplesPerTrigger',inf);

%Setting up data logging modes and file name to log data into

%files

set(ai,'LoggingMode','Disk'); set(ai,'LogToDiskMode','Index');

set(ai,'LogFileName','data.daq');
```

The next step is to filter the signal. A Finite Impulse Response (FIR) low pass filter is used in this case. It is a 50th order filter designed using a Hamming window. The magnitude and the phase response of the filter is shown in Figure 3.22. The frequency scale is normalized by the sampling frequency where the cut-off frequency 0.0625 corresponds to 25Hz. The last step of this process involves downsampling or decimating the data by a factor of 4.
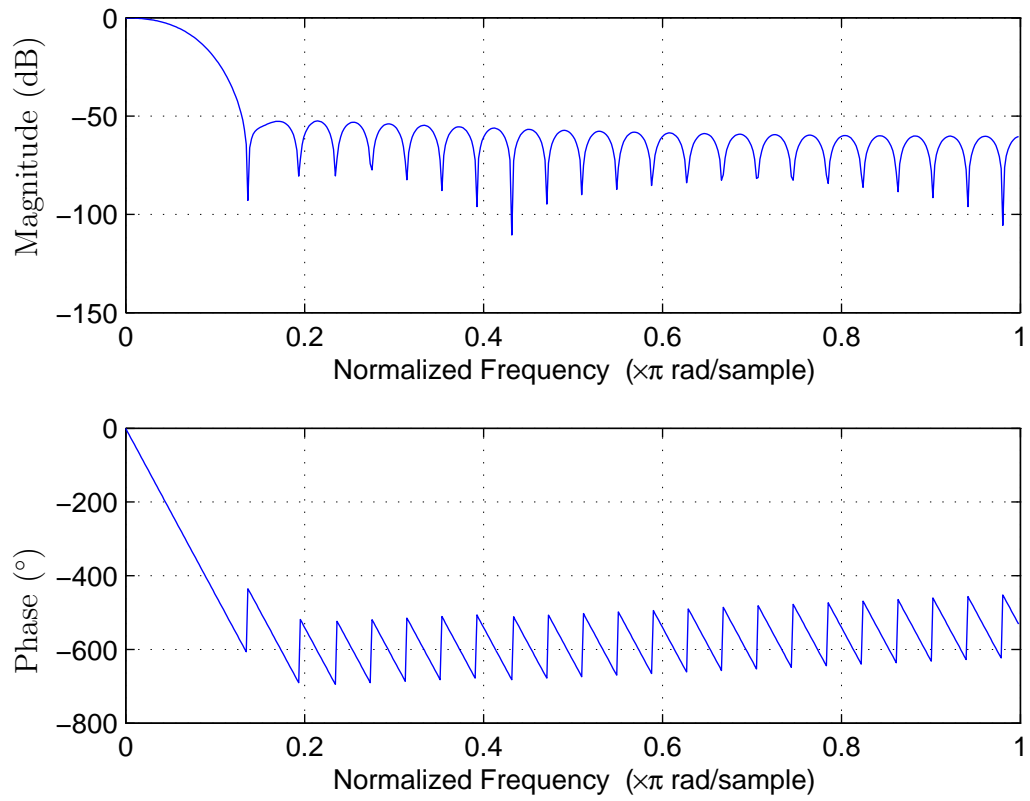
Figure 3.22: Magnitude and phase response of the FIR low pass filter.

4.   Evaluation of the Dead Reckoning Sensor System

In this chapter, the evaluation tests performed on the dead reckoning sensor system and the corresponding results are presented. Initially a test setup is described and then the analysis is presented using the following few steps.

1. data collection through sensors,

2. sensor data processing,

3. data integration and comparison

4.1   Test Location

The evaluation tests are performed inside the engineering building of the University of Saskatchewan. The system of hallways within the building provides a test environment that is similar to the tunnel like structures in mines. A digital map, which was programmed in MATLAB, was used for the test and it is shown in Figure 4.1. This map represents a portion of the main floor in the College of Engineering building. On the map, the (0,0) co-ordinate is indicated with a shaded square. Since the main floor is considered horizontal to the earth's surface, the third axis (z) is not used in the analysis. The map is drawn to scale and smaller details are ignored in the map. However, for the mining applications, detailed digital mine maps are drawn using programs such as Autocad or Gocad. In these digital mine maps, tunnels are expressed in a three dimensional planar system.
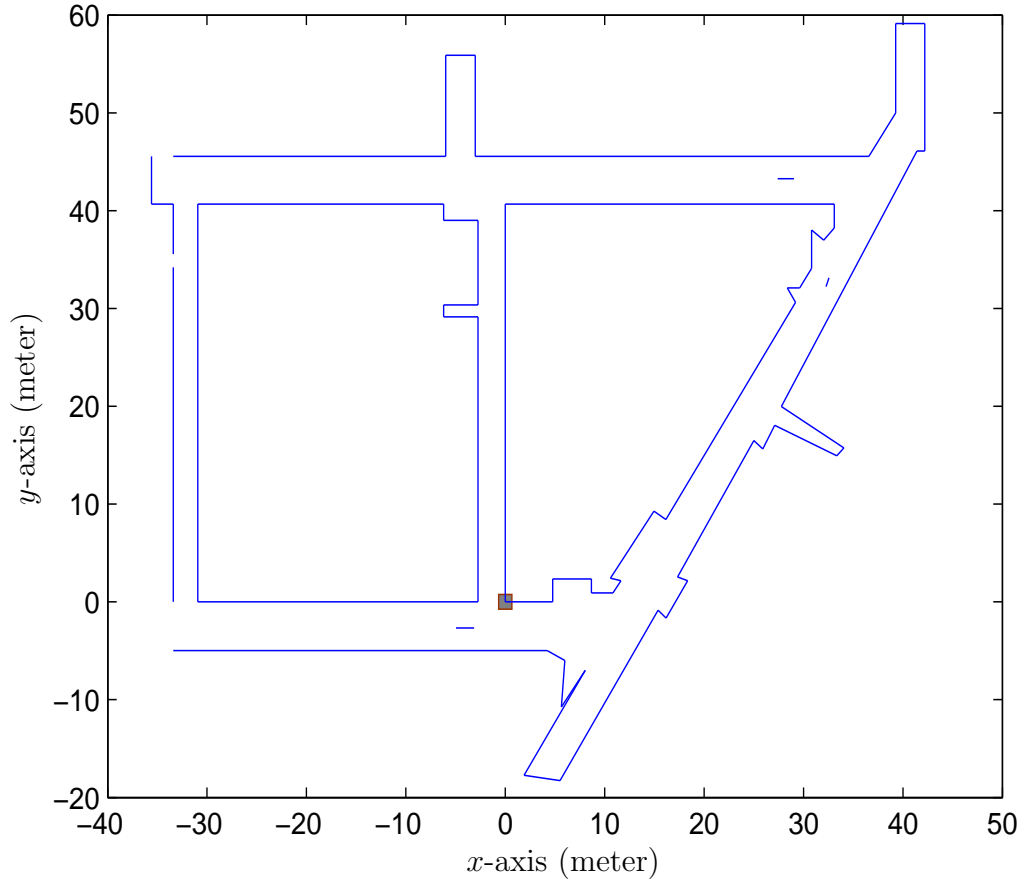
Figure 4.1: Map of hallways inside engineering building

4.2   Test Equipment

A wagon was used for the test. The equipment was mounted on the wagon as shown in Figure 4.2. The equipment used for this test includes a battery, a laptop computer, the dead reckoning sensors, a power supply, an power inverter and a data acquisition board. As shown in Figure 4.3, the dead reckoning sensors include two ultrasound sensors, a rate gyroscope and a dual axis accelerometer. The axis of the forward direction accelerometer was parallel with the base of the wagon and pointed in the same direction as the wagon's handle. The DC power from a 12 volt car

Figure 4.2: Equipment in wagon

Rate
Gyroscope

Dual Axis
Accelerom-
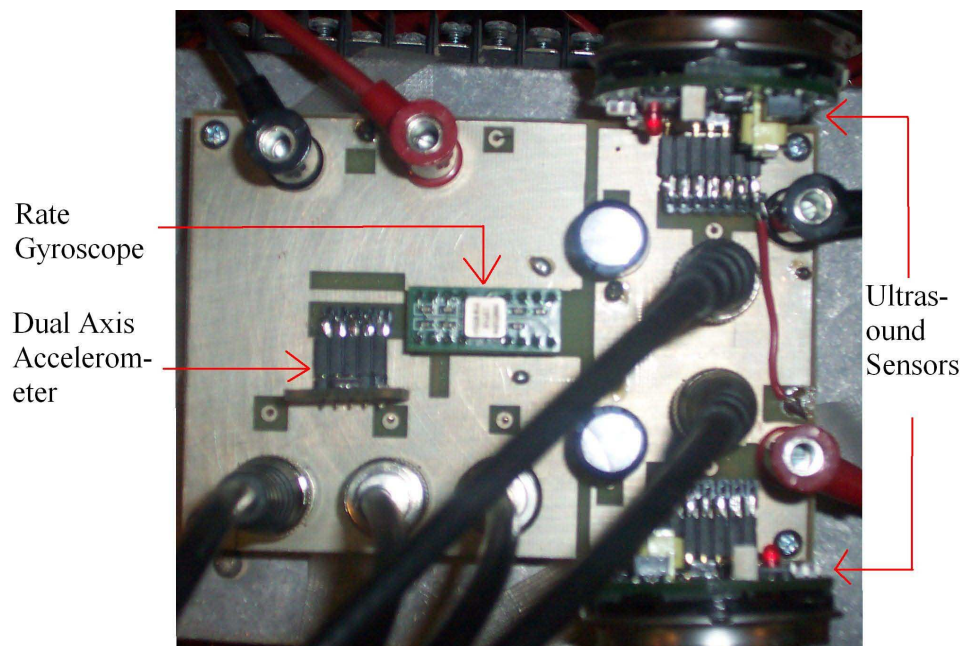eter

Ultras-
ound
Sensors

Figure 4.3: Sensor Board

battery was converted to 110 volts AC by the inverter. The laptop computer and a dual regulated DC power supply were connected to the inverter. The dual regulated

DC power supply provides power to the sensors at two different voltage levels, since the MEMS sensors require a supply voltage of 5 Volts and the ultrasound sensors require 10 Volts.

The wagon was pulled manually through the hallways inside the building. A picture of one of the hallways is shown in Figure 4.4. The hallways were confined by side walls, but occasionally there were openings to other hallways and rooms. The wagon was pulled by its handle and the path shown in the map of Figure 4.5 was followed. The starting point was the (0,0) coordinate marked by shaded rectangle and the wagon followed the dashed line.

Figure 4.4: One of the hallways where the testing was done

4.3 Data Collection

Initially the wagon was at rest. After the power supplies for the sensors were turned on there was a delay of a few minutes to give the sensors the time to warm up and stabilize their output level. After the warm up period was over, the laptop computer started to collect data through the data acquisition system with the help of the Matlab data acquisition toolbox. The wagon was pulled along the path shown in Figure 4.5.
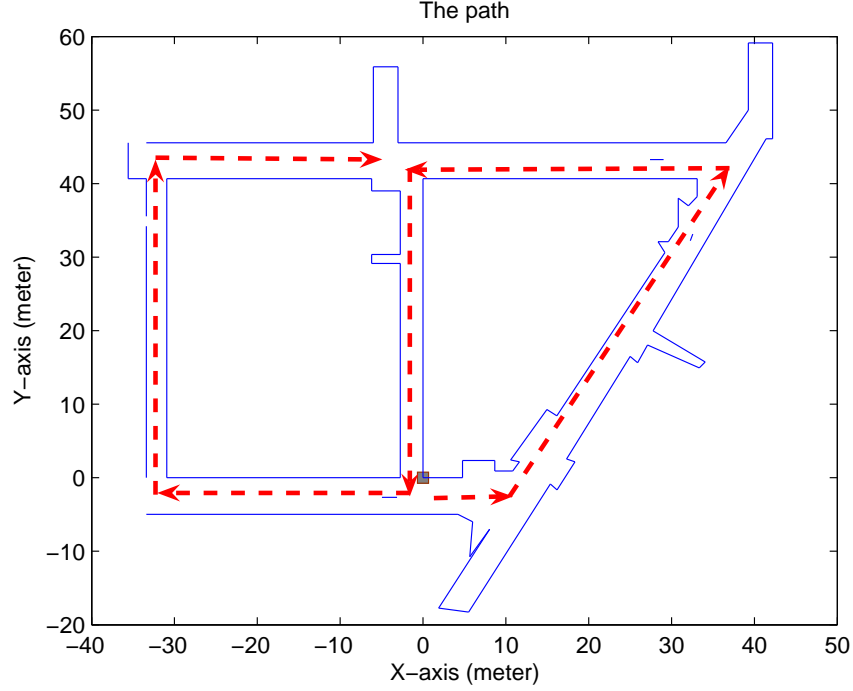
Figure 4.5: Direction of travel through hallways inside engineering building

4.4 Data Processing

Data acquired by the laptop computer is a sampled version of the analog signals from the sensors. Figure 4.6 shows one second of collected data (includes offset voltages). The sampled data must be processed to determine the information relating to the position of the vehicle.

For example, data collected from the forward direction accelerometer can be transformed to determine the distance traveled by the wagon. Accumulated distance, $d[n]$ for each sampled forward direction acceleration, $a_f[n]$ was calculated using,

$$s[n] = s[n-1] + a_f[n] \times \triangle t \tag{4.1}$$

and

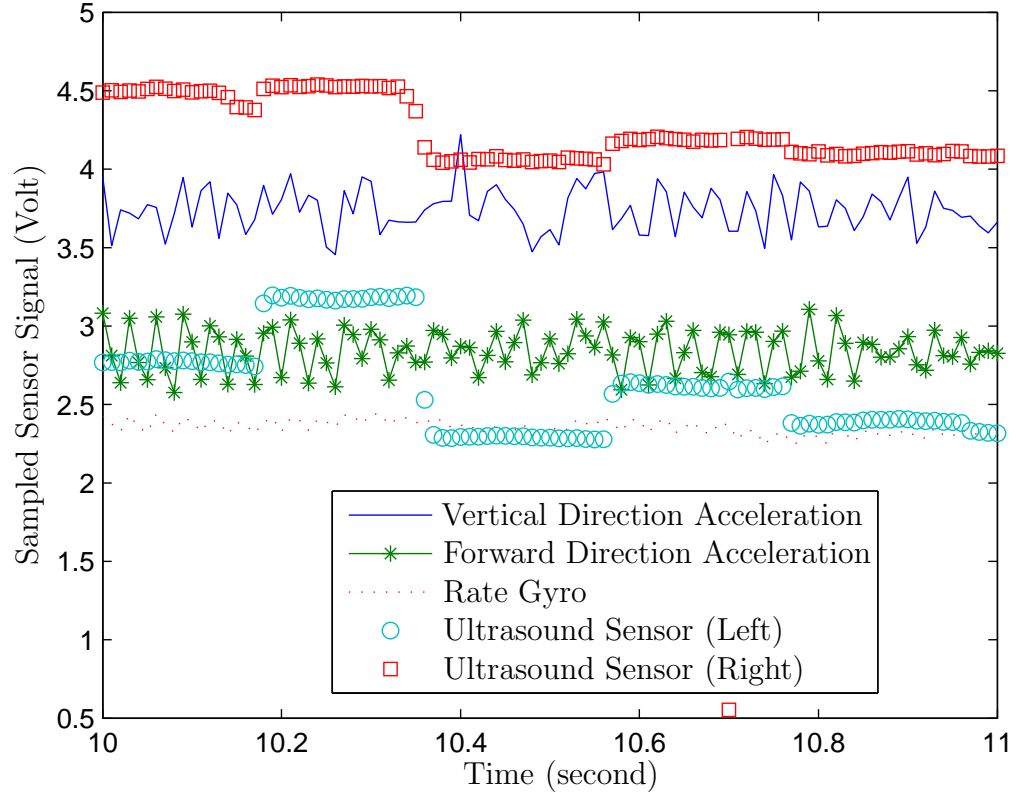$$d[n] = d[n-1] + s[n] \times \triangle t + 1/2 \times a_f[n] \times (\triangle t)^2 \tag{4.2}$$

Figure 4.6: One second of collected data from the sensors through data acquisition system with some offset voltage

where $n = 1, 2, 3....$ is the sample number, $s[n]$ is the speed at nth sample and $\triangle t$ is the time difference between two samples. Initial speed $s[0] = 0$ meter/sec. For this experiment, data from the acceleromter is transformed to give distances and the plot of the result is given in Figure 4.7. In this plot, beside the measured distance (dotted line), the calculated expected distance (solid line) is also given. The time stamps were logged when the wagon reached to a certain landmark position such as an opening by looking at the ultrasound data. The expected distance from one landmark position to another was calculated for that time period. The plot indicates that there was
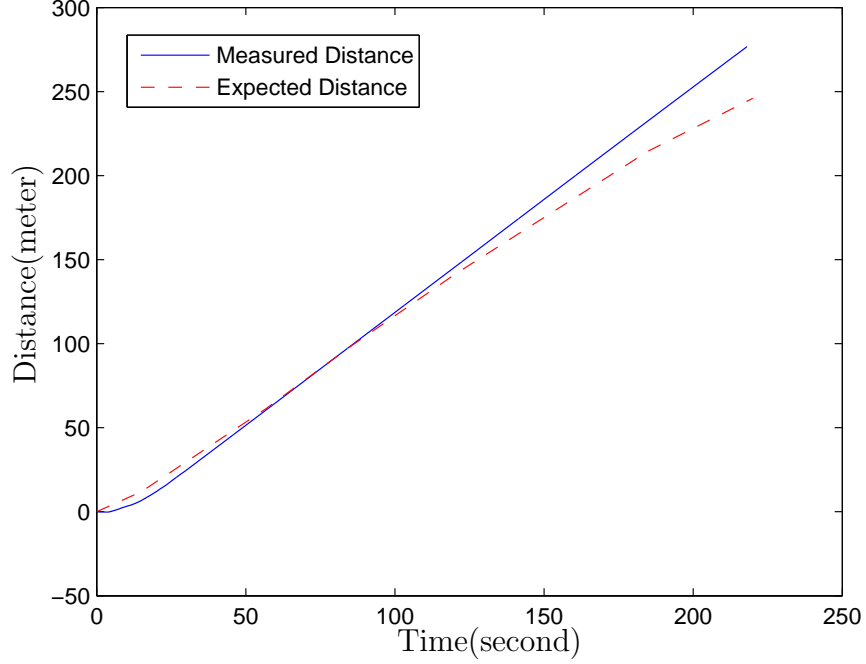
Figure 4.7: Calculated distance for the path.

some error in the measurement. The calculated distance from the measured data was greater than the expected distance due to the presence of bias and scale factor.

A similar transformation is required for the rate gyro data. The sampled signal from the rate gyroscope, which is in volts, is divided by the sensitivity, converting it to unit of °/second. The converted signal gives the change of bearing angle, $\dot{\theta}[n]$ °/second. The bearing $\theta[n]$ represents direction of the wagon relative to initial position at each sample. $\theta[n]$ was calculated using the equation

$$\theta[n] = \theta[n-1] + \dot{\theta}[n] \times \triangle t \tag{4.3}$$

where $\theta[0] = 0°$ for the initial position. Figure 4.8 shows the wagon's bearing angle in degrees. The figure shows both the measured and expected bearing angle. The expected angles were calculated from the map and correlated with time stamps when
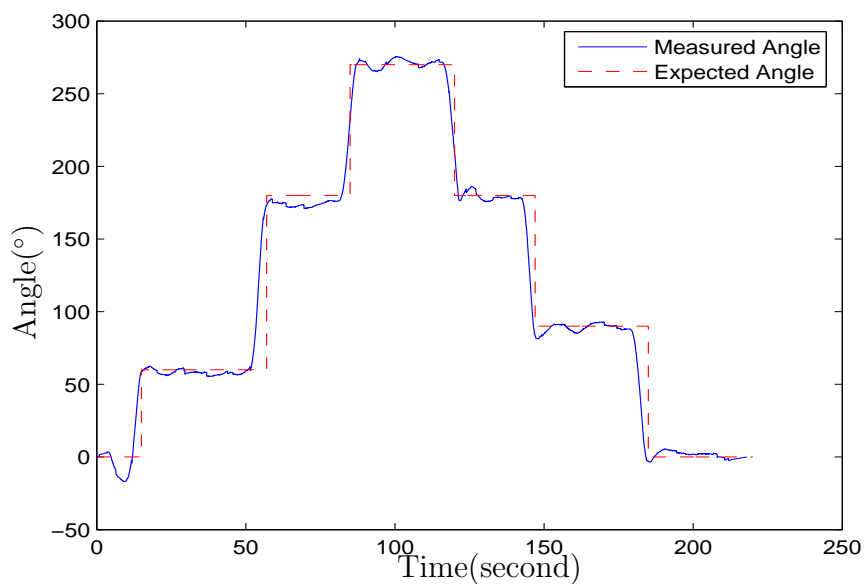
64

Figure 4.8: Direction of the wagon while it was traveling through the hallways

the wagon passed certain landmarks. It is apparent there is a good correspondence between the measured and expected angle.

Lastly, the sampled voltage signal from the two ultrasound sensors were transformed to distance by dividing by the sensitivity. In Figure 4.9, distance from side walls is shown from the 10th to 40th second of traveling time. A distance close to 10 meters at the 5th second indicates that there was an opening to another hallway. This is marked with a circle on the plot. The ups and downs of distance from the side walls from the 20th to the 35th second indicate changes of width of the hallways.

4.5   Data Integration and Comparison

The transformed data, which provides the forward distance, the bearing angle and the distances from side walls, can be combined to generate the path that the wagon was pulled through. The transformed data from the accelerometer and rate
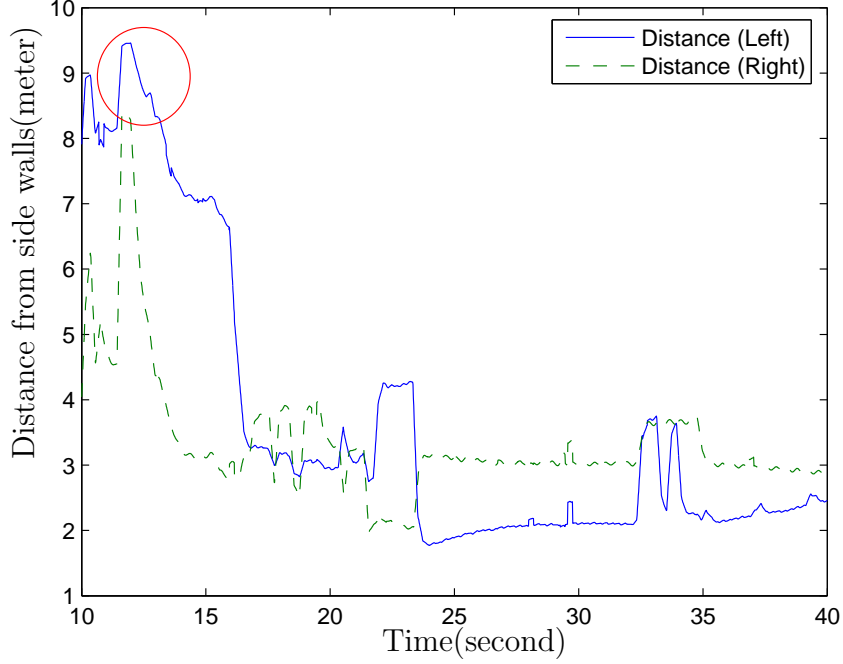
Figure 4.9: Distance from side walls.

gyroscope are combined for this purpose. The equations that are used to combine the information from these two sensors to find the (x, y) coordinate of the wagon are

$$x[n] = x[n-1] + (d[n] - d[n-1])(\cos(\theta[n])) \qquad (4.4)$$

and

$$y[n] = y[n-1] + (d[n] - d[n-1])(\sin(\theta[n])), \qquad (4.5)$$

where $d[n]$ is the accumulated distance travelled by the wagon until the nth sample point and $\theta[n]$ is bearing angle at the nth sample point relative to the initial reference point. At the reference point (0,0), $d[n] = 0$ meter and $\theta[n] = 0°$. Combining the accelerometer and rate gyroscope data gives a plot of the path travelled that is shown in Figure 4.10.

Data from ultrasound sensors are combined with the data from acceleromter and
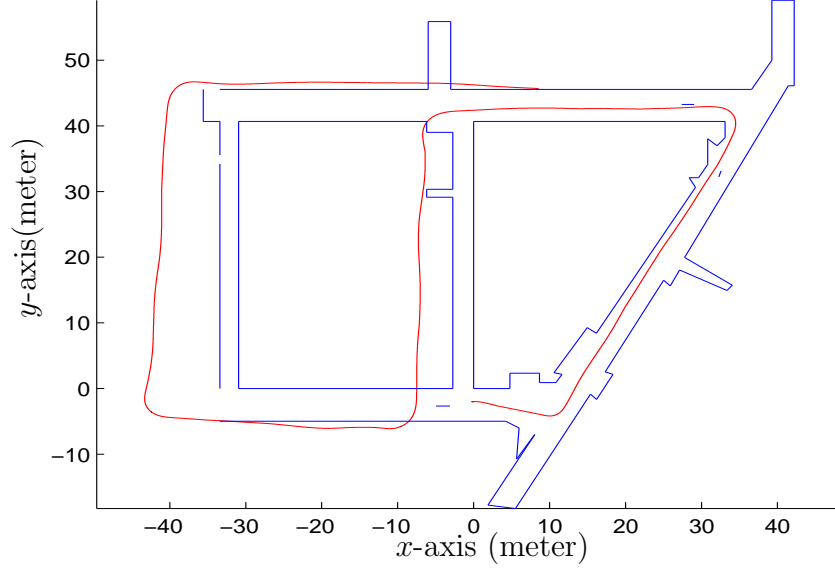
66

Figure 4.10: Path travelled using combined accelerometer and gyroscope

rate gyroscope. Combining the data from all of these sensors gives a plot of the left and right side walls shown in Figure 4.11. This was calculated using the (x, y) coordinates found from Equation (4.4) and (4.5), the distance from the left side wall, D_{left} and the distance from right side wall, D_{right}. This information was used in the following equations to calculate the coordinates of the left side walls $(x_{left}[n], y_{left}[n])$ and coordinate of the right side walls $(x_{right}[n], y_{right}][n])$

$$x_{left}[n] = x[n] - D_{left} \sin(\theta[n]) \tag{4.6}$$

$$y_{left}[n] = y[n] + D_{left} \cos(\theta[n]) \tag{4.7}$$

and

$$x_{right}[n] = x[n] + D_{right} \sin(\theta[n]) \tag{4.8}$$

$$y_{right}[n] = y[n] - D_{right} \cos(\theta[n]) \tag{4.9}$$

In this analysis, only the data from the dead reckoning system is used to find
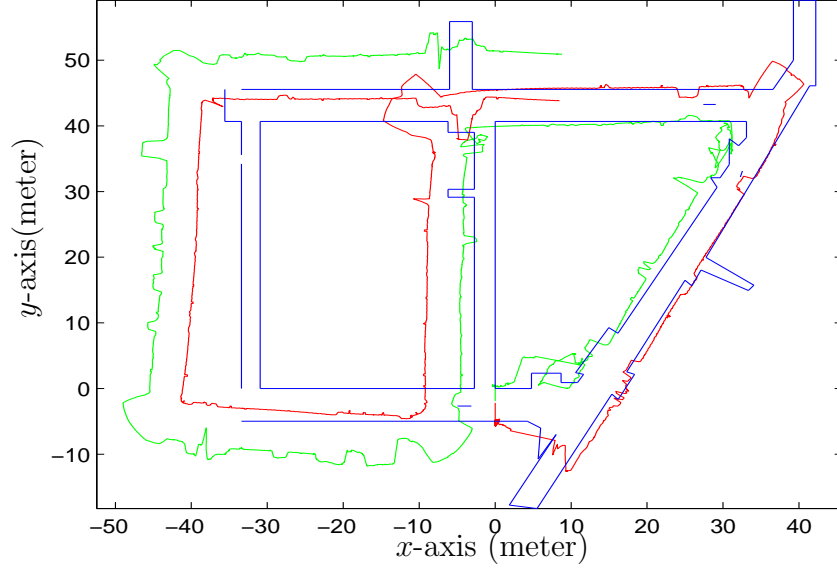
67

Figure 4.11: The location of the left and the right side walls were calculated using Equation (4.6), (4.7), (4.8) and (4.9)

the position of the wagon. The data fusion algorithm was not used to calculate the position. Figure 4.10 clearly shows that for a given initial position, the position of the object becomes less accurate with time due to accumulation errors in the sensor data. Therefore the necessity of the data fusion algorithm becomes clear. It is needed to adjust the position of the object or the vehicle with time more accurately. For example, when the vehicle makes a turn to another passage, it could use the digital map to improve the location estimate. The information relating to the digital maps is provided by the ultrasound distance sensor. This information when integrated with the accelerometer and rate gyroscope data using a data fusion algorithm can provide a better location estimate.

A simplified example is given in Figure 4.12. At the point marked by the circle, the wagon took a left a turn. Had the algorithm adjusted the wagon's position to the
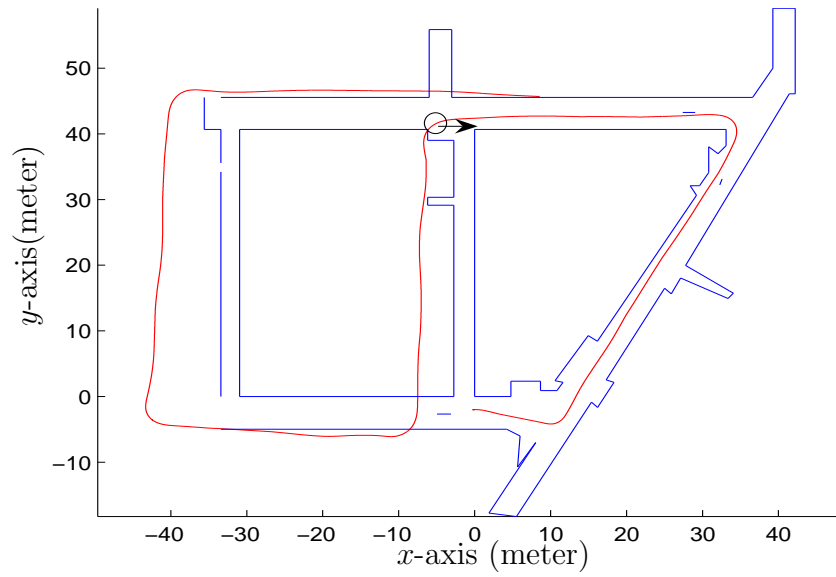
Figure 4.12: Position that needs to be adjusted is marked by a circle
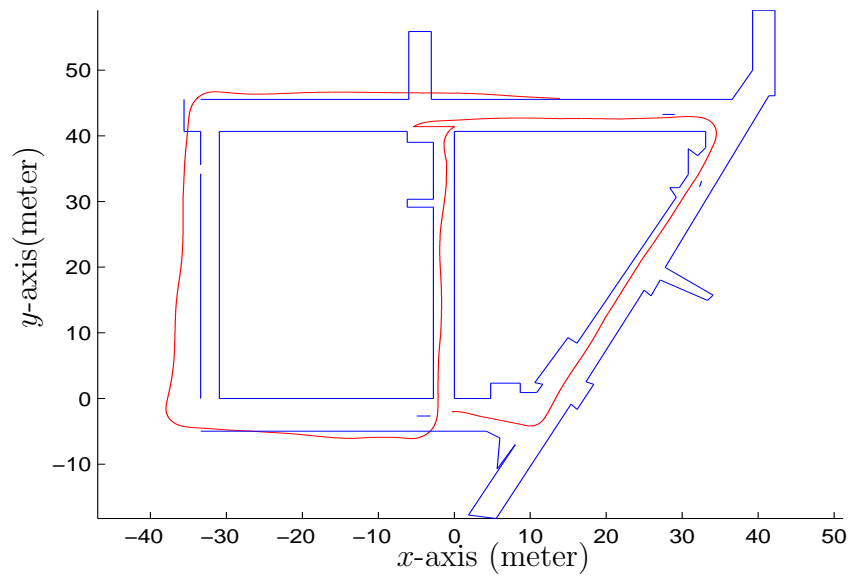
Figure 4.13: Position of the wagon is adjusted to match with the map

69

point indicated by the arrow, it would have improved the overall position accuracy as shown in Figure 4.13. Similar adjustments continuously applied throughout the path would find the position of the wagon more accurately. Since the implementation of algorithm is still in the development process, the system's performance could not be tested using the actual algorithm.

5. SUMMARY AND CONCLUSIONS

The intent of this research was to investigate and design a dead reckoning system, which could estimate the relative position of a vehicle. The system had to be suitable for underground mines. The research also involved the evaluation of the sensors which were used to build the dead reckoning system. This dead reckoning system will be integrated with a statistical data fusion algorithm to locate mobile objects inside mine tunnels. Although there are various types of dead reckoning systems, the one that was chosen for this research was based on prioritizing cost, reliability, suitability with the environment inside mines and moreover to support the particle filter based data fusion algorithm. Even though various types of sensors and dead reckoning system were considered, only the kind of system and its elements, which was finally selected, were discussed in this thesis.

The dead reckoning system had three main parts: the sensor block, the data acquisition block and the interface that provides data to the algorithm. The sensor block had four types of sensors: accelerometer, gyroscope, speed and distance sensors.

The dual axis accelerometer had one axis in the forward direction and another one in the downward direction relative to direction of travel. Before mounting on to the vehicle, analysis was done by setting up an experimental pendulum testbed. The experiment characterized the bias and scale factors.

An experimental test setup was also generated for the rate gyro to investigate the accuracy. Since the aim was to measure the angle while the vehicle was turning, a similar experiment was performed. The result was close to expected angle with an

average error of 1.43%.

Tests on ultrasonic distance sensors also showed that they were able to measure distances from side walls with an error of less than 10 cm. Although a speed sensor would provide additional information for the data fusion the algorithm, it is not included in the current dead reckoning system. Measurements from all of these sensors were made available through the data acquisition system and improvements in accuracy were made by reducing the noise in the sampled signal.

An example test was done inside a tunnel in the engineering building, where measurements were taken from the dead reckoning sensor system. Measured voltage signals were sampled by the data acquisition system and later transformed to distance units. The data from the various sensors was combined to make comparisons between the expected and measured vehicle path values. Finally the research indicates that significant improvement can be made in the location estimate by using the digital map in a data fusion algorithm.

5.1 Future Work

There are several tasks that need to be done to complete the requirement of the proposed in-mine positioning system. The first task is to test data acquired from the dead reckoning system with the data fusion algorithm implemented in another M.Sc. project. The second task is the development of a Radio Frequency reference beacon system to give the initial position estimate. The long term objective is to extend this work to provide positioning information anywhere in mine and in any other tunnel like structures, including train and automotive tunnels. The final task involves performance tests that must done on the complete positioning system at a mine location.

In the future, it should be noted that ADXL203 is most sensitive when its sensitive axis is perpendicular to the force of gravity, and less sensitive when its sensitive axis is parallel to the force of gravity. For future evaluation method, one suggestion can be made. Instead of collecting the time stamps when the vehicle reach to some landmark positions from sensor data, the time stamps should be collected independently by using a stop watch.

References

[1] C. Reid Ferring, Paul Goldberg, Vance T. Holliday, "Earth sciences and archaeology," pp. 363–65, 2000.

[2] S. S. Saab, "A map matching approach for train positioning. part I: development and analysis," *IEEE Transactions on Vehicular Technology*, vol. 49, pp. 467–475, March 2000.

[3] D. H. Titterton, J. L. Weston, *Strapdown Inertial Navigation Technology*, vol. 207, Progress in Astrnautics and Aeronautics, 2nd edition, 2004.

[4] Honeywell, *Ring Laser Gyro*, Online document: http://content.honeywell.com/dses/products/gyros/.

[5] Crossbow, *Pilot Guide*, Online document: http://www.xbow.com/General_info/gyro_guide.htm.

[6] OBDII, *On-Board Diagnostic systems*, Online document: http://www.obdii.com/.

[7] Arnaud Doucet, Nando de Freitas, Neil Gordon, *Sequential Monte Carlo Methods in Practice*, Springer, 2001.

[8] Stefan Ahlqvist, Fredrik Gustafsson Urban Forssell, Peter Hall, "Map-aided positioning system," 2002.

[9] Warren Hawkins, Brian Daku, Arfin F. Prugger, *Positioning in Underground Mines*, IEEE Industrial Electronics, IECON 2006 - 32nd Annual Conference, 2006.

[10] Angus F.C. Errington, Brian L.F. Daku, Arfin F. Prugger, "Vehicle positioning in underground mines," CCECE, 2007.

[11] D. Fox, *Kld-sampling: Adaptive particles filters and mobile robot localization*, University of Washington, Department of Computer Science and Engineering, 2002.

[12] M. Bolic, "Architecture for efficient implementation of particle filters," 2004.

[13] Nebot E., *Sensors used for autonomaous navigation*, Kluwer Academic Publisher, Dordrecht, 1999.

[14] Analog Devices, *Data sheet for Accelerometer Sensor ADXL203*, Online document: http://www.analog.com/UploadedFiles/ data_Sheets/ 279349530ADXL103_203_0.pdf.

[15] Charles Kitchin, *Understanding Accelerometer Scale and Offset Adjustment*, Application Note, AN-396, Analog Devices.

[16] James Stewart, *Calculus*, Brooks/Cole Publishing Company, 1999.

[17] Wikipedia, *Least Squares*, http://en.wikipedia.org/wiki/Least_squares, 2006.

[18] SensComp, "600 series environment transducer," *Online Specification Sheet: http://www.acroname.com/ robotics/parts/R134-600.pdf*, July 2003.

[19] John Geen, David Krakauer, "New imems angular-rate-sensing gyroscope," *Analog Devices-Analog Dialogue*, vol. 37, March 2003.

[20] Analog Devices, *Data sheet for Angular Rate Sensor ADXRS150*, Online document: http://www.analog.com/UploadedFiles/ Data_Sheets/ 778386516ADXRS150_B.pdf.

[21] National Instruments, *DAQCard E-series user manual*, Online document: http://www.ni.com/pdf/manuals/321138a.pdf, 1996.

[22] Woon-Seng Gan M. Kuo, *Digital Signal Processors*, Prentice-Hall, Inc., 1999.

[23] Leonard Staller, "Improving a/d converter resolution by oversampling and averaging," *ChipCeter Questlink*, 2003.

[24] John R. Buck, Alan V. Oppenheim, Ronald W. Schafer, *Discrete-Time Signal Processing*, Prentice-Hall, Inc., 2004.

A. APPENDIX A

A.1 Coriolis Effect

In physics, the Coriolis effect is an apparent deflection of moving objects when they are viewed from a rotating frame of reference.

The effect is named after Gaspard-Gustave Coriolis, a French scientist who described it in 1835, though the mathematics appeared in the tidal equations of Pierre-Simon Laplace in 1778. The Coriolis effect is caused by the Coriolis force, which appears in the equation of motion of an object in a rotating frame of reference. The Coriolis force is an example of a fictitious force (or pseudo force), because it does not appear when the motion is expressed in an inertial frame of reference, in which the motion of an object is explained by the real impressed forces, together with inertia. In a rotating frame, the Coriolis force, which depends on the velocity of the moving object, and centrifugal force, which does not depend on the velocity of the moving object, are needed in the equation to correctly describe the motion.

Perhaps the most commonly encountered rotating reference frame is the Earth. Freely moving objects on the surface of the Earth experience a Coriolis force, and appear to veer to the right in the northern hemisphere, and to the left in the southern. Movements of air in the atmosphere and water in the ocean are notable examples of this behavior: rather than flowing directly from areas of high pressure to low pressure, as they would on a non-rotating planet, winds and currents tend to flow to the right (left) of this direction north (south) of the equator. This effect is responsible for the rotation of large cyclones (see Coriolis effects in meteorology).

In non-vector terms: at a given rate of rotation of the observer, the magnitude of the Coriolis acceleration of the object is proportional to the velocity of the object and also to the sine of the angle between the direction of movement of the object and the axis of rotation.

The vector formula for the magnitude and direction the Coriolis acceleration is

$$a_c = -2\Omega \times v \tag{A.1}$$

where v is the velocity of the particle in the rotating system, and Ω is the angular velocity vector which has magnitude equal to the rotation rate w and is directed along the axis of rotation of the rotating reference frame, and the $\times$ symbol represents the cross product operator.

The equation may be multiplied by the mass, m of the relevant object to produce the Coriolis force:

$$F_c = -2m\Omega \times v \tag{A.2}$$

The Coriolis effect is the behavior added by the Coriolis acceleration. The formula implies that the Coriolis acceleration is perpendicular both to the direction of the velocity of the moving mass and to the frame's rotation axis. So in particular:

- if the velocity is parallel to the rotation axis, the Coriolis acceleration is zero

- if the velocity is straight inward to the axis, the acceleration is in the direction of local rotation

- if the velocity is straight outward from the axis, the acceleration is against the direction of local rotation

- if the velocity is in the direction of local rotation, the acceleration is outward from the axis

- if the velocity is against the direction of local rotation, the acceleration is inward to the axis